The Thesis Committee for Hao Wu
Certifies that this is the approved version of the following thesis:

Functional Nanocomposite Fibers through Electrospinning: Flame Retardant and Superhydrophobic

APPROVED BY
SUPERVISING COMMITTEE:

Supervisor: _____
Mourad Krifa

Co-Supervisor: _____
Joseph H. Koo

Functional Nanocomposite Fibers through Electrospinning: Flame Retardant and Superhydrophobic

by

Hao Wu, BE

Thesis

Presented to the Faculty of the Graduate School of

The University of Texas at Austin

in Partial Fulfillment

of the Requirements

for the Degree of

Master of Science in Textile and Apparel Technology

The University of Texas at Austin

May 2012

Acknowledgements

First, I would like to thank Dr. Mourad Krifa and Dr. Joseph H. Koo for their teachings during my two year study in the University of Texas at Austin. This thesis would not have been possible without their guidance.

I would also like to thank Dr. Jonathan Chen from Textile and Apparel department, Dr. Donald Paul from Chemical Engineering, Dr. Holly Stretz from Tennessee Tech University, and Dr. Jitendra S. Tate from Texas State University for their abundant help and invaluable assistance.

Special thanks to my lab mates and friends Lakshmi Padmaraj, Xiaoli Yin, Chunhong Lu, and colleagues Dickson Lao, Swapnil Gaikwad, and Preejith Ambuken. Sincere gratitude also goes to Dr. Hugo Celio, Dr. Shouliang Zhang, and Mr. Jeff Cook from Texas Materials Institute (TMI), and Dr. Damon Smith and Dr. Joshua Bolinger from Center for Nano and Molecular Science (CNM) for their patient training and help in experiments.

Finally and most importantly, I want to thank my family, especially my parents and grandparents for their great love and continuous support throughout my life.

Abstract

Functional nanocomposite fibers through electrospinning: flame retardant and superhydrophobic

Hao Wu, MSTAT.

The University of Texas at Austin, 2012

Supervisor: Mourad Krifa, Joseph H. Koo

Flame retardant (FR) intumescent additives and montmorillonite (MMT) organoclay incorporated nylon-6 nanocomposite (FR-NC-PA6) fibers with a diameter of about 200 nm were fabricated by electrospinning. Before electrospinning, dispersion and exfoliation of the FR additive and MMT in nylon-6 were achieved by twin-screw extrusion. Tensile, TGA and UL-94 flammability tests were first performed using injection-molded bulk samples. The tensile modulus of FR-NC-PA6 was 45% higher than that of neat PA6, but tensile strength and elongation at break decreased by 23% and 98.7%, respectively. It is worth noting that although the TGA results show that FR-NC-PA6 has a slightly earlier decomposition temperature than neat PA6, it did not drip under fire and had the best rating (V-0) in UL 94 test, while neat PA6 is only rated as V-2. SEM and EDX of char residues after the UL 94 test clearly show the oxygen-rich protective char layer on the surface. These results indicate the advantage of using clay and FR additive in bulk-form PA6.

Flammability of electrospun nanocomposite fibers was characterized by Micro-combustion calorimeter (MCC), a small-scale test to screen flammability of polymer materials. The MCC results show that the nano-fillers in both bulk and fiber form could effectively improve flame retardant properties of the material. Electrospun fibers had similar combustion properties as bulk materials.

In addition to FR applications, superhydrophobic surface was another area that was explored using the electrospun nanocomposite fibers. Static water contact angle (WCA) test showed that samples with 5wt% clay even without plasma treatment greatly improved the WCA to 140°, probably due to the barrier effect of nanoclay platelets. Plasma treatment was used to modify the surface energy, further improving WCA to as high as 160°. However, fiber structure was partially etched away when overexposed to the plasma. This etching effect increased the surface roughness. Clay incorporated samples had higher level of surface roughness and better resistance to plasma etching compared to neat nylon 6.

Table of Contents

List of Tables

List of Figures

Chapter I: Introduction

1.1 Motivation

There are growing concerns regarding health and safety issues of workers and soldiers who frequently encounter harsh environments. Therefore regulations and standards on the performance of their apparel have been enforced [1]. This led to continuous development of personal protective equipment (PPE) that includes protective clothing and gears, such as respirators, face masks, etc. Based on different applications, protective clothing can be categorized into chemical protection, thermal protection, radiation protection, biological protection, and mechanical protection. It became widely used in controlled environments, such as laboratory clean room users, and by emergency response personnel including firefighters, military, and police.

Fire protection is one of the major functions of protective clothing. Various types of high performance fibers, such as Nomex®, Twaron® and Polybenzimidazole (PBI) have been developed to provide effective fire protection. In order to provide enough protection from the environment, conventional protective clothing is often made of bulky multi-layer or laminated fabrics with poor permeability to air and water vapor. Beyond that, these high performance fibers are not as cost effective as other widely used synthetic fibers such as polyethylene and nylon. Thus current protective clothing systems are still not common in mass produced performance apparel market.

Another interesting area that has drawn significant research attention is self-cleaning or surperhydrophobic fabrics where the surface of the fabric is super repellent to water and or other chemicals. Inspired by the water repellent lotus leaf, this technology can be applied in protective clothing for chemical and biological protection. It can also be

used for high performance sportswear where no stain would attach to the surface while still maintaining good permeability to air and water vapor.

In this study, we explore the process of electrospinning combined with the concept of polymer nanocomposites as a feasible way of making both flame retardant (FR) and self-cleaning fibers using conventional synthetic fiber materials and non-toxic fillers.

1.2 Background

On December 29th, 1959, Dr. Richard Feynman made a visionary statement at the American Physical Society (APS) conference at the California Institute of Technology, saying that "There's plenty of room at the bottom" [2]. From that moment, a new era concentrated on "nanotechnology" was initiated. The National Science Foundation defines nanotechnology as "research and technology development at the atomic, molecular or macromolecular levels, in the length scale of approximately 1-100 nanometer range, to provide a fundamental understanding of phenomena and materials at the nanoscale and to create and use structures, devices and systems that have novel properties and functions because of their small and/or intermediate size" [3]. Several key features of nanomaterial such as quantum effect, large surface to volume ratio and controllable wetting behavior are utilized by engineers from different disciplines. A perfect example would be as the concerns for depletion of fossil becomes prevalent, solar energy is one of the most reliable and promising energy resources to be developed. Taking advantage of their high surface area, nanomaterials could be engineered to make high efficiency solar cells [4-7]. Depending on the geometry of the material, nanomaterials can be classified as "zero-dimensional" systems such as quantum dots,

"one-dimensional" systems, such as nanowires, nanotubes and nanofibers and "two-dimensional" systems such as graphene [8].

Among those structures, nanofibers drew particular attention. The reason is that when fiber diameter goes down to sub-microns or nanometers, defects within fibers will be largely reduced. It has also been shown that the crystalline structure could be altered by processing materials into nanofibers [9], which will result in higher fiber strength. Such nanofibers have been intensively studied for applications in filter media, tissue engineering, fuel cell electrodes, and optical sensors [10-13]. It is worth to mention that although the definition by NSF requires one dimension to be less than 100 nm, in actual practice the term "nanofibers" is usually accepted over a broader range which includes dimensions that are smaller than 1000 nm or 1 μm.

For years, a number of techniques have been developed to make nanofibers, including drawing, template synthesis, phase separation, self-assembly, electrospinning, etc.[11]. The drawing method is similar to that of the traditional fiber spinning process where the raw materials are melted or dissolved and single fiber are formed by pulling or stretching. Fibers made by this method usually have good orientation and thus high strength; but only a material with good enough elasticity and viscosity could withstand large deformation [14]. Template synthesis uses a membrane with nanopores to extrude materials into fiber form. This method was used to make carbon nanofibers and nanotubes by chemical vapor deposition within pores of alumina template membranes [15]. Phase separation is composed of several stages including dissolution, gelation and extraction that will render a foam structure with nanoscale pores[16]. However, it takes a relatively long time for the foam to be formed. Self-assembly is a method widely used in fabricating nanowires from which components are organized into certain patterns; but this method also have its limitations due to difficulty to produce continuous fibers in

large scale [17, 18]. Other than the methods mentioned above, several processing techniques were designed for some particular materials. For example, air-blast atomization of mesophase pitch could produce large quantities of non-woven fibers quickly [10]. However, the disadvantage is that it can only produce short fibers and the material choice is also limited.

1.2.1 ELECTROSPINNING

Electrospinning, originally known as "electrostatic spinning", first appeared in the early 20th century. The technique utilizes a strong electric field to draw a spinning jet from polymer solutions up to 1,000 times across a short distance and time duration. The core parts of an electrospinning apparatus is shown in Figure 1. This method is widely used to produce random or aligned nanofibers with diameters typically ranging from tens to hundreds of nanometers. Electrospinning nanofibers from a broad range of polymers are an area of research that has drawn significant attention in recent years because of the exceptional properties of nanostructured materials.

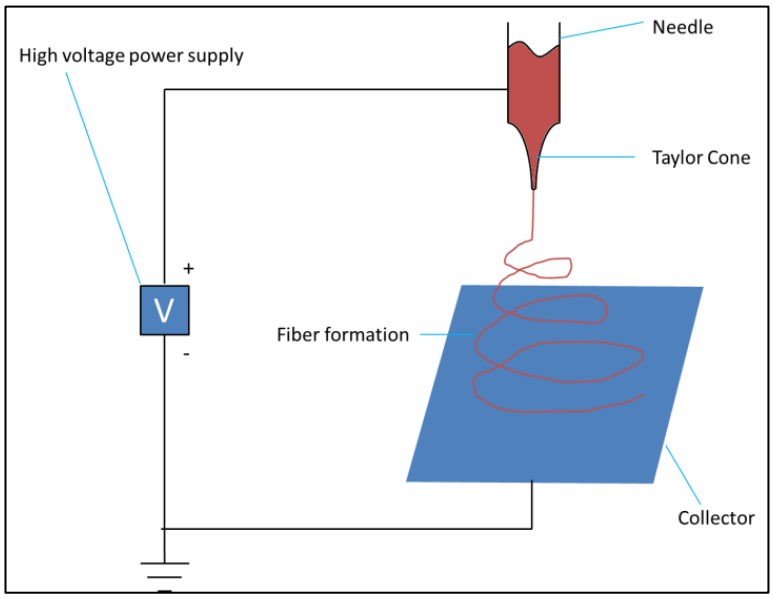

Figure 1. Schematic of electrospinning process.

The electrostatic repulsive force will overcome the surface tension on the droplet surface, solution jets will be ejected from the tip of the conically deformed droplet toward a grounded collector [19]. The electrostatic force on the surface of the extruded solution jet stretches it into a circular fiber shape, and the solution solidifies as the solvent evaporates into air. Because of the high specific surface area, this evaporation process is very rapid.

Although this phenomenon has been discovered a long time ago, the principle and mechanics behind it are rather complicated. Studies have shown that solution properties, such as shear viscosity, polymer concentration, solution conductivity, surface tension, and elasticity, will have an influence on fiber morphology. Yu originally summarized all the different factors that play a role in determining the final fiber morphologies [20]. Here we further sorted these factors into 3 categories namely: fluid properties, processing parameters, and combinatorial factors, as shown in Figure 2.

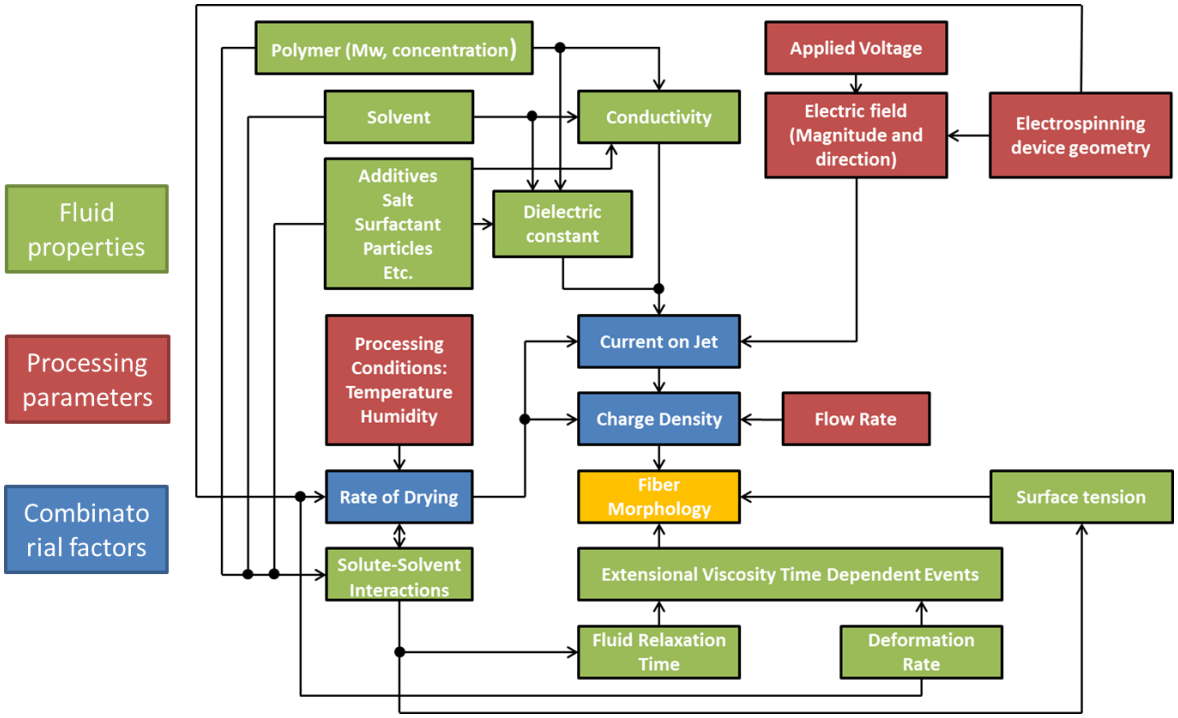

Figure 2. Summary of factors affecting the fiber morphology.

1.2.2 Polymer Nanocomposites

Polymer nanocomposites (PNC) are materials with nanofillers dispersed in the polymer matrix. These nanofillers usually act as reinforcement to the polymer matrix. It was found that remarkable enhancement in properties, such as mechanical, thermal, electrical or chemical could be achieved by even small amounts of nanofillers.

Since the Toyota group successfully made clay/nylon 6 nanocomposites by in-situ polymerization, Polymer-clay nanocomposites have been extensively studied during the last decade due to their improvement in mechanical, thermal, and biodegradability properties [21-26]. One of the most useful applications of nanocomposites is in the area of flame retardant materials, i.e. flame retardant coatings for electronics and electrical

equipment, and protective textiles [27, 28]. Among different varieties of clays, montmorillonite (MMT) is one of the most commonly used nanofillers in polymer nanocomposite. It has a large surface area providing plenty of interfacial regions in the polymer matrix, which allows for an enhancement of thermal and mechanical properties at low weight percentage [29, 30]. MMT clay has a plate structure (Figure 3) which consists of an octahedral layer sandwiched between two silicate tetrahedral layers [30]. The octahedral layer in the middle is composed of an aluminum oxide sheet in which some aluminum atoms are replaced by magnesium. This composition variation created negative charges in the sheet and the charges are balanced by positive ions, such as sodium ions between the platelets [30]. MMT clays have an irregular shape in the range of 100-200 nm in lateral direction; the thickness of single layer is about 1nm [31].

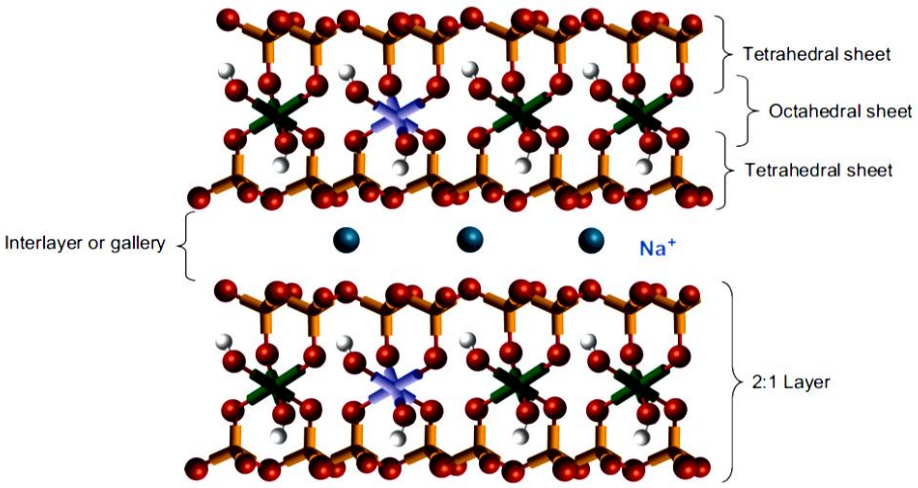

Figure 3. Structure of MMT clay (Reproduced with permission of Ref.[30]).

Study on MMT nanocomposites have shown that one of the most important factors affecting the properties of polymer-clay nanocomposites is the degree of dispersion of clay particles [24]. Pristine MMT are not compatible with polymer matrix

therefore surface modification is needed to attain high level of dispersion. Organic surface modification of clay is usually carried out by ion exchange reactions with primary, secondary, tertiary, and quaternary alkylammonium or alkylphosphonium action in the interlayer spacing; this reaction will decrease the surface energy of the inorganic host and improve the affinity with the polymer matrix. The exfoliation of silicate layers can be achieved by in situ polymerization or polymer melt-extrusion. Paul et al. [30, 32] showed that PA6 has a good affinity with modified silicate surfaces, and therefore high levels of exfoliation can be achieved [24].

1.3 Objectives

This thesis is divided into two parts based on two application scenarios both related to protective clothing, i.e. flame retardant and self-cleaning. The first part explored the possibility of making flame retardant nylon 6 nanofibers for the potential use as a low cost substitute or component of laminate fire proof fabrics. In this section, flame retardant additives and nanoclay will be added to the neat polymer system to make electrospinning solutions. Mechanical properties, thermal, and flame retardant properties will be characterized.

The second part will be focused on self-cleaning properties of nanofiber mats where the morphology modification was achieved both internally and externally. The internal modification was by adding small amount of nanoclay into the system where nanoclay platelets will increase the surface roughness of the fibers. External modification was achieved by plasma deposition of a thin layer of low surface energy material on the fiber surface. Static water contact angle and AFM will be used to characterize the superhydrophobic samples.

Chapter 2 Ultra-thin Flame Retardant Nylon 6 Nanocomposite Fibers

2.1 Introduction to Flame Retardant Nanocomposites

Military, firefighting personnel, and some civilians, such as infants need effective protection from fire threats. Currently a number of high performance flame retardant fibers such as Nomex®, and PBI are widely used in firefighter and racer suits due to their excellent fire resistance. However, when it comes to large scale production these materials are not as cost effective as other commonly used polymers like nylon or polyester. Extensive studies have shown that nylon 6-intumescent-clay nanocomposite systems are not only an effective flame retardant but also very cost effective [21, 30]. Moreover, synergism effects of clay and intumescent flame retardant additives could help to further enhance flame retardant performance. With the addition of intumescent systems, the self-sustained combustion of the polymer will be interrupted at an early stage. The mechanism behind the intumescence process is that charring and foaming on the surface of the burning polymer will form. This foamed cellular charred layer, the density of which decreases as a function of temperature, protects the underlying material from the action of the heat flux or the flame [33-35].

2.2 Experimental Methods

2.2.1 Materials

Low/medium viscosity Nylon 6 (Aegis® H8202NLB) was provided by Honeywell Co. Formic acid (>88%) was purchased from Sigma-Aldrich Chemical Co. The nanoparticle filler used in this study is Montmorillonite nanoclay Cloisite® 30B from Southern Clay Products Inc. Cloisite® 30B is a natural montmorillonite modified

with a quaternary ammonium salt ME2EtOH. It is an additive used in plastics to improve various plastic physical properties such as reinforcement, heat deflection temperature (HDT), coefficient of linear thermal expansion (CLTE), and barrier property[36]. Flame Retardant additives Exolit® OP1312 were provided by Clariant Ltd. Exolit OP 1312 is a non-halogenated flame retardant additive based on organic phosphinates. The flame retardant mechanism is through intumescence where the thermoplastic polymers such as nylon 6 with OP1312 will foam and crosslink on exposure to flame and form a stable char at the surface acting as a barrier. The protective layer provides a heat insulation effect, reduces oxygen access, and prevents dripping of molten polymer [37]. OP1312 were wet milled in ethanol by NETZSCH Premier Technologies, LLC before use. Nylon 6, nanoclay, and FR were all dried at 80^{o}C for at least 24 hours before processing.

2.2.2 Experimental Design

The goal of this study is to make ultra-thin flame retardant nanocomposite fibers by electrospinning. Two methods of compounding for making electrospinnable fluids were proposed (Figure 4). Twin screw extrusion has been proven to be an effective method for polymer mixing. Using this method, a fine dispersion of both clay and FR can be achieved. DSM microcompounder is a type of batch mixer that has been reported by Chavarria et al. as comparable to twin screw extrusion to mix polymers and nanoparticles in small quantities (around 3g/batch) [38]. Thus, the first method we used was high shear mixing using twin screw extrusion/DSM microcompounder to premix the polymer with nanoclay (NC) and flame retardant (FR) additives before dissolving in formic acid. Another method was to directly mix polymer and additives in the solvent without premixing. Properties of these samples in terms of morphological, thermal, and flame retardant characteristics were compared. Based on previous experiments [33-35], twin

screw extruded samples containing 20wt% FR and 5wt% NC will render desirable flame retardant properties on bulk material. However, it was found that the electrospinning fluids have poor electrospinnability with such high portion of fillers. In order to improve electrospinnability, formulations with lower filler concentrations were attempted using different mixing methods as discussed above. A more detailed discussion of electrospinnability will be given in section 2.2.3.3. All samples formulated in this study are shown in Table 1.

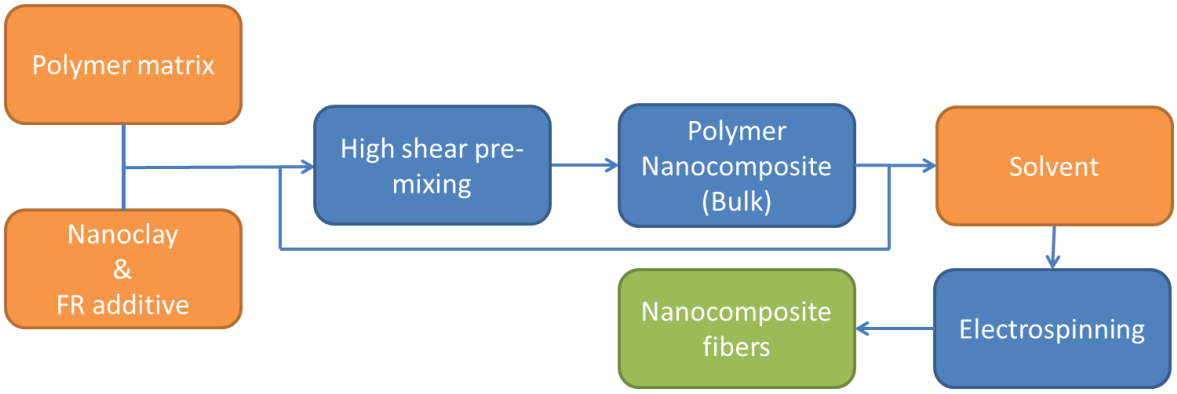

Figure 4. Schematic flow chart of experimental design.

Table 1 Formulations and their composition

	Sample#	PA6	FR	Clay
Control	1	100	-	-
Solution blending	2	85	15	-
	3	80	15	5
	4	80	20	-
	5	80	17.5	2.5
High shear pre-mixing	6	75	20	5
	7	80	15	5
	8	80	20	-

2.2.3 Fabrication

2.2.3.1 Pre-mixing of Nanofillers in Polymer Matrix

One of the key factors is to obtain a good dispersion of nanofillers in the polymer solution. As discussed above, three methods were used to prepare the electrospinning fluid and compared in terms of electrospinnability and flame retardant properties. These two methods are listed as follows:

- High shear melt compounding: 3 g of polymer and additives were fed into DSM microcompounder each time. The rotation of the screw was 100 rpm and compounding time was 3 min at 240°C.
- Solution blending: Particles including nanoclay and FR additives were mixed in nylon 6 by solely solution blending. Solutions containing different loadings of particles were blended using magnetic stirrer for 12 hours.

2.2.3.2 Electrospinning

Electrospinning solutions were prepared by dissolving 20wt% of solid compound with formic acid and gently stirring with a magnetic stirrer at room temperature. Both neat PA6 nanofiber mats and nanocomposite fibers were produced using the same electrospinning parameters (voltage, distance, feeding rate, etc.) as shown in Table 2.

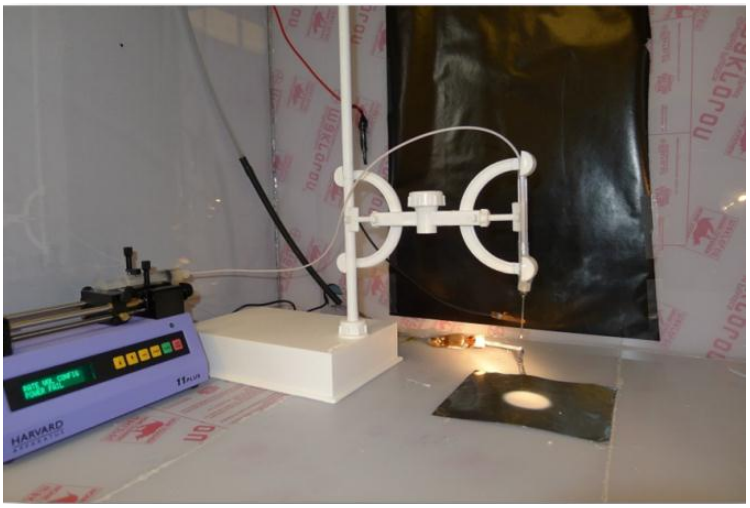

Figure 5. Electrospinning apparatus.

Table 2 Electrospinning parameters

Voltage	25±1kV
Collecting distance	8±1cm
Feeding rate	4±1$\mu l/min$
Solute concentration	20%, 25%, 30%

The solutions were electrospun into fibers using a lab-built electrospinning apparatus (as illustrated in Figure 1and Figure 5). The solutions were fed at a rate of 4±1 $\mu l/min$ using a syringe pump (Harvard Apparatus, 11 Plus) connected to an 18 Gauge needle (Harvard Apparatus); the collecting distance was 8±1 cm. The needle tip was connected to a high voltage power supply (Gamma High Voltage Research, ES 100P-10W/DAM). The voltage was set to 25±2 kV. The parameters were slightly adjusted each time to obtain a stabilized polymer jet forming the fiber mats. A piece of grounded aluminum foil (15 cm by 15 cm) was used to collect the fiber mats. The electrospun fibers were carefully cut and removed from the surface by peeling.

2.2.3.3 Electrospinnability

The term "electospinnability" refers to the ability for a polymer solution to be electrospun into fibers with uniform morphology. Elasticity and viscosity of the fluid are two important factors that influence electrospinnability [20]. When elasticity is not sufficient or viscosity is too high to withstand the stretching during spinning, droplets or beads on a string structure will be formed instead of uniform fibers. This phenomenon is a common problematic issue in this study where high concentrations of nanofillers like nanoclay will be more likely to form droplets or beads on string fibers. This poor electrospinnability is due to the "Raleigh instability" driven by surface tension of the fluids. According to Yu [20], this "Raleigh instability" can happen in the steady jet region or the whipping region. It is commonly found that fluids with high filler concentrations are likely to form droplets and low concentration of polymer in solvent will form beads on string structure due to Raleigh instability and the lack of elasticity.

Here we define electrospinnability in a descriptive manner: for a fluid having desirable electrospinnability, there must be no observable break ups during the spinning process. Fiber diameter should be uniform throughout the whole sample with minimal/no droplet or bead formation.

2.2.3.4 General Electrospinning Procedure

The general electrospinning procedure is summarized as follows:

1. Clean apparatus making sure there is no dust in the fume hood;

2. Check instrument power is plugged in properly and keep power off;

3. Fill syringe with compounded solution, be careful not to induce air bubbles;

4. Remove air bubbles by reducing pressure in the syringe (e.g., put in vacuum oven);
5. Attach one end of Teflon tube to the syringe through female luer lock, attach the other end to a male luer lock;
6. Place the syringe in the syringe pump;
7. Assemble Teflon tube onto the iron stand;
8. Attach stainless steel needle to the Teflon tube through the male luer lock;
9. Connect high voltage supply wire to the needle, making sure it's well connected;
10. Set the initial flow rate to 200-300$\mu l/min$, reduce the rate to desired level around $5-10\ \mu l/min$ when fluid reaches the needle;
11. Thoroughly clean the needle tip with acetone/water;
12. Turn on the voltage power supply immediately after the needle is cleaned, set the voltage to around 25kV;
13. Adjust the voltage and distance to ensure stable spinning jet;
14. If there is dry drop formation at the needle tip, turn off power supply and ground the apparatus before cleaning;
15. When finished, zero voltage indicator before turning off the power supply;
16. Collect residual fluid into a recycling container;
17. Dispose of the Teflon tube and luer lock, clean the needle thoroughly using blow torch or formic acid.

2.3 CHARACTERIZATION

The morphology of the electrospun fibers was observed by Scanning Electron Microscopy (SEM, Hitachi S-5500 and Quanta 650) equipped with Energy-dispersive X-ray spectroscopy (EDX). SEM and EDX analyses were also performed on the char

residues of extruded sample bars after the UL 94 tests (see 2.4.5). Due to surface charging, electrospun fibers, and char samples were sputter coated with Pt/Pd prior to observation.

For bulk material characterization, twin-screw extruded nanocomposite pellets were dried and injection-molded into standard tensile bars (ASTM D638, Type I) [39]. Tensile tests were performed using an Instron 3345 (Instron, Inc.) with a 5kN load cell equipped with an extensometer. All specimens were conditioned for 48 hours before testing. The gauge length was 115 mm, and cross-head speed was 5 mm/min. The reported Young's modulus, ultimate strength, and ultimate strain for tensile bars were the average values of 5 tests.

Thermal properties of injection-molded films were characterized by thermogravimetric analysis (TGA-50, Shimadzu Corporation) in nitrogen at a flow rate of 20 cc/min and a heating rate of 10°C/min. All samples were heated up to 80°C and held for 10 min to erase previous thermal histories, and then returned to room temperature for a full scan.

Flammability of injection-molded samples was evaluated by the UL 94 test. UL 94 is a standard, small-scale flame test for flammability of plastic materials. Thermal combustion properties of both injection-molded films and electrospun fibers were measured using a microscale combustion calorimeter (MCC2, Govmark, Inc.) according to ASTM D7309-2007. First developed by the U.S. Federal Aviation Administration (FAA), MCC is a technique that could quantitatively evaluate flammability by directly measure heat release rate of small amounts of materials in the size of milligrams. This technique perfectly fits the needs to test the flammability of ultrathin fibers where it would be very costly and time-consuming to produce large samples. The samples were

heated at a heating rate of 1°C/sec to 700°C in the apparatus. Each sample was tested in 3 repetitions to ensure accuracy.

2.4 RESULTS AND DISCUSSIONS

2.4.1 Mechanical Properties of Twin-Screw Extruded Bulk Material

With 5wt% clay and 20wt% FR additives, the rupture tensile strength of bulk sample #6 decreased by about 23% compared to the control (sample #1), while Young's modulus increased by 45% (Figure 6 and Table 3). The enhancement in Young's modulus can be explained by the nucleation effect of clay, in which higher crystallinity was formed in nylon 6 during processing [40]. Usuki et al. found that montmorillonite interacted strongly with nylon 6 by ionic interactions [41]. This ionic interaction might be one of the reasons why these hybrid materials had superior stiffness, i.e. higher modulus. However, the elongation at break of formulation #6 is substantially lower than the control. This phenomenon is in agreement with results obtained on nylon 11 with similar additive compositions [33]. The decrease in tensile strength and elongation at break may be due to poor interfacial bonding between MMT and FR particles within the PA6 matrix.

Table 3 Tensile properties of bulk #1 and #6

Sample(bulk)	**Ultimate Tensile Strength (MPa)**		**Tensile Modulus(MPa)**		**Elongation at break (%)**	
	Average	SD	Average	SD	Average	SD
#1	59.3	2.8	1436	72	230	33
#6	45.4	1.1	2685	103	3.1	0.3

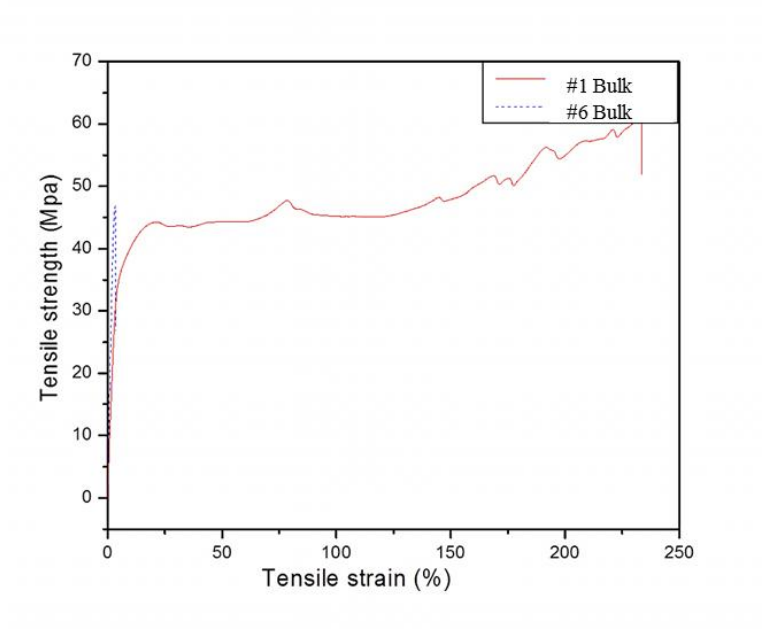

Figure 6. Stress strain curve of bulk samples #1(PA6) and #6 (FR-NC-PA6).

2.4.2 Thermal Properties of Twin Screw Extruded Bulk Materials

TGA was performed on hot pressed bulk samples #1 and #6 under nitrogen flow. The mass loss behavior of the two samples is shown in Figure 7. No significantly different onset degradation temperature was observed between that of neat PA6 (#1) and #6. In all cases, the nanocomposite formulation #6 possesses lower decomposition temperatures than neat PA6. The temperatures at 50% mass loss are 458-473°C for #1 and 434-453°C for #6 (Table 4). Single stage decomposition was observed for both samples (Figure 8) and formulation #6 had a lower peak mass loss rate than #1. Moreover, the difference in residue weight after decomposition was significant. While the char residue left was close to zero in the case of the control formulation (#1), it increased to around 20% in the case of the #6 nanocomposite formulation.

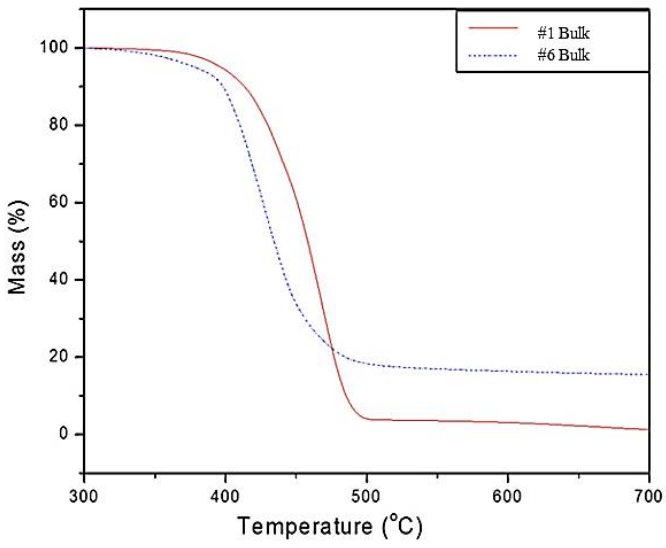

Figure 7. TGA curves of bulk #1and #6 (10°C/min).

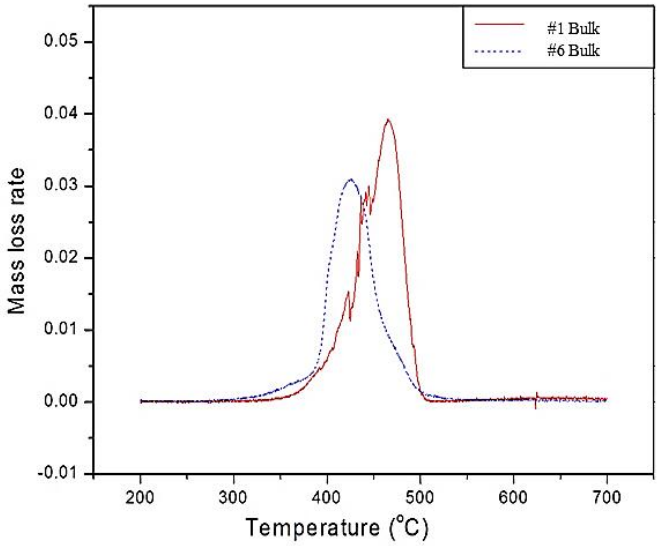

Figure 8. Mass loss rate of #1 and #6 (10°C/min).

Table 4 TGA 5wt%, 10wt%, and 50wt% loss for bulk #1 and #6

Sample (bulk)	$T_{5wt\%}$(10 °C /min)	$T_{10wt\%}$(10 °C /min)	$T_{50wt\%}$(10 °C /min)	$T_{5wt\%}$(20 °C /min)	$T_{10wt\%}$(20 °C /min)	$T_{50wt\%}$(20 °C /min)
#1	396	413	458	409	426	473
#6	373	397	434	391	411	453

2.4.3 Thermal Properties of Electrospun Fibers by Solution Blending

Thermal stability of electrospun fibers by solution blending were characterized by TGA with same heating rate in nitrogen flow. The TGA curves shown in Figure 9 appear rather different from those of twin-screw extruded samples. What's in common is that with addition of FR or NC with FR, the samples tend to start degrading at lower

temperatures than neat PA6. However, mass loss rate curves (Figure 10) reveal that solution blended samples have three obvious peaks whereas neat PA6 only have 1 major peak. The overall mass loss rates were effectively decreased by adding FR and NC. Furthermore, as indicated in Figure 10, it appears that higher FR wt% results in higher peaks at low temperatures (approx. 340°C) corresponding to the degradation of FR additives, and lower peaks between 400°C and 500°C where nylon 6 degrades. Similar results were also found for DSM blended electrospun fibers, as shown in Figure and Figure 12, where the composite samples start to degrade at a lower temperature but overall mass loss rate was reduced significantly.

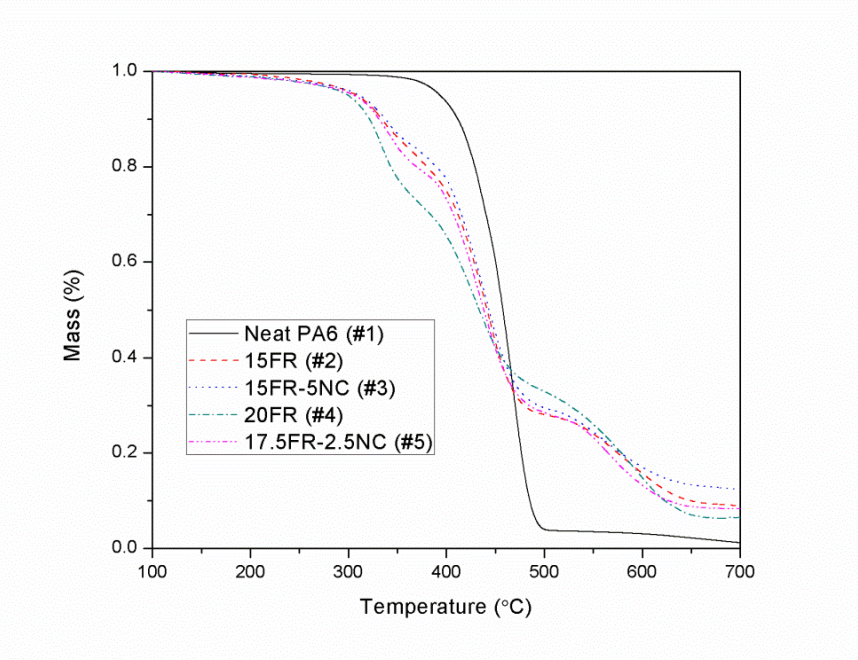

Figure 9. TGA of solution blended electrospun fibers (10°C/min).

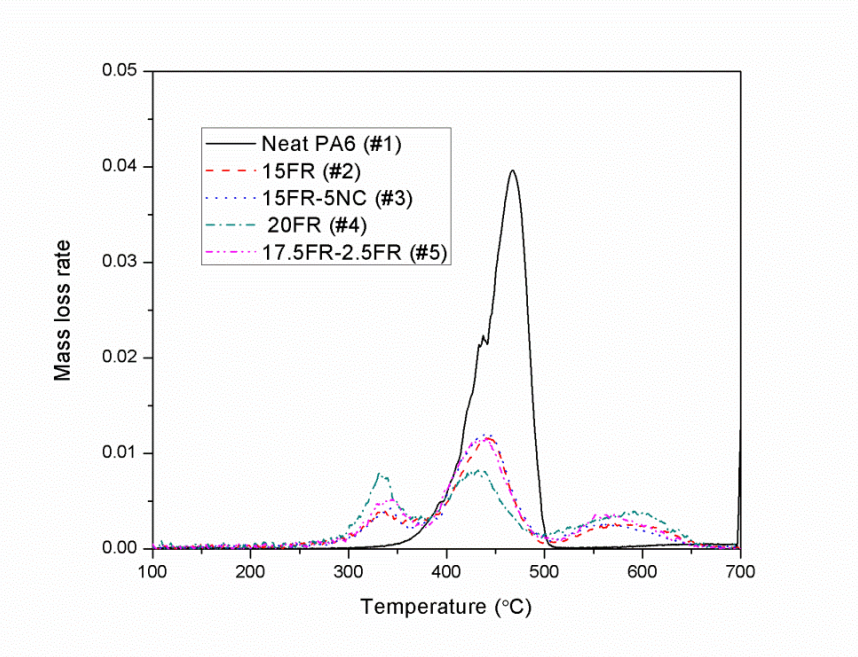

Figure 10. Mass loss rate of solution blended electrospun fibers (10°C/min).

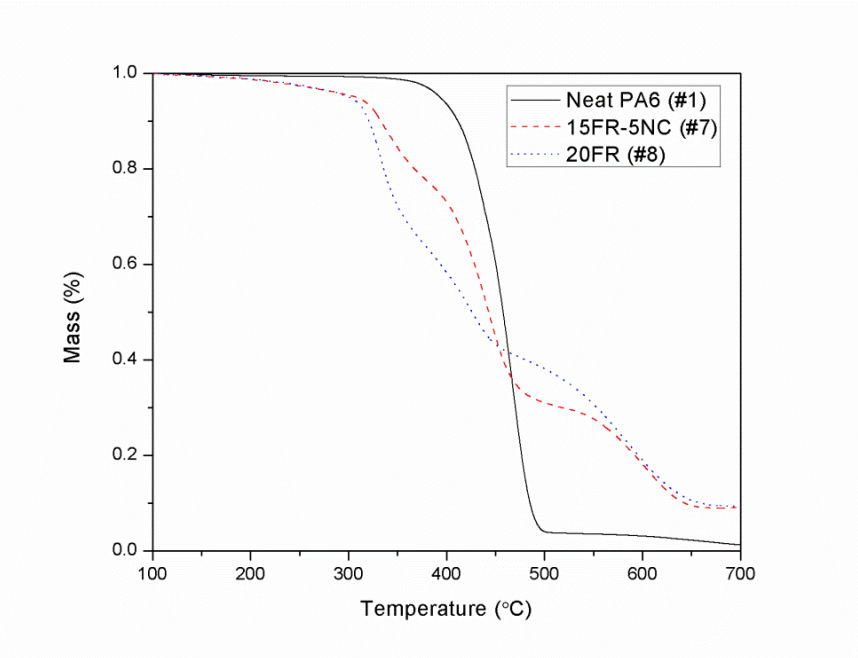

Figure 11. TGA of melt blended electrospun fibers (10°C/min).

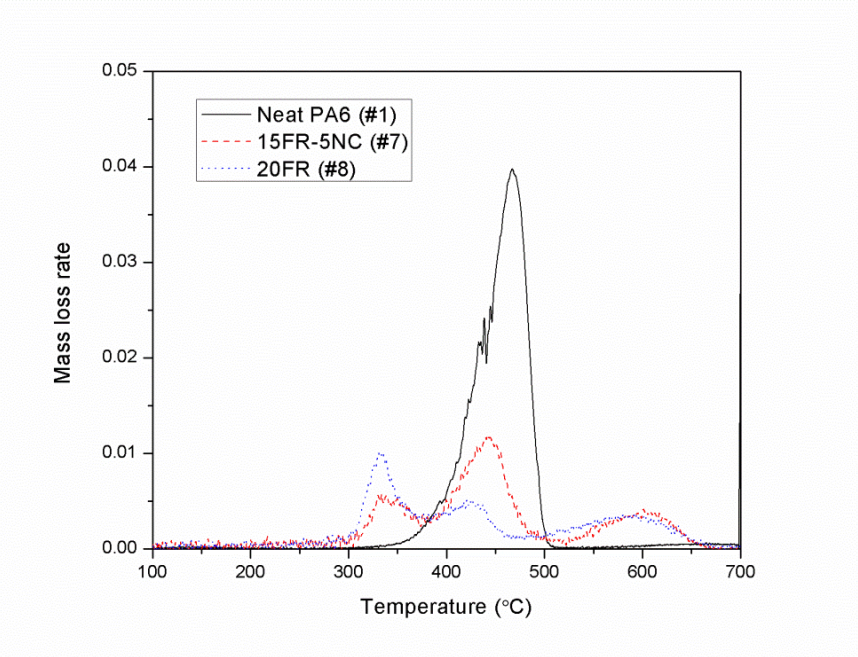

Figure 12. Mass loss rate of DSM blended electrospun fibers (10°C/min).

2.4.4 Flammability of Twin Screw Extruded Bulk Materials (UL 94)

In the UL 94 test, PA6 control sample bars (#1) burned for more than 10s after the first flame application; they also dripped as shown in Figure 13(a) and ignited the cotton indicator. Therefore, sample #1 was rated as UL 94 V-2. As for bulk #6, it immediately ceased burning after removal of the flame. There was only a very short period of glowing after the second flame application. No obvious shape deformation was observed for #6, except for a small expansion from the surface of the sample, as illustrated in Figure 13(b). The expansion may be due to the addition of intumescent flame retardant additives. All the #6 sample bars passed UL 94 V-0.

The difference in UL 94 results shows an obvious enhancement of flame retardant performance when PA6 is mixed with FR and nanoclay. Interestingly, this result does not

correlate to the decreased thermal degradation temperatures observed in TGA results. TGA does show, however, increased char residue, which is a good indication for enhanced flammability properties. Char residue characterization is discussed in 2.4.5.

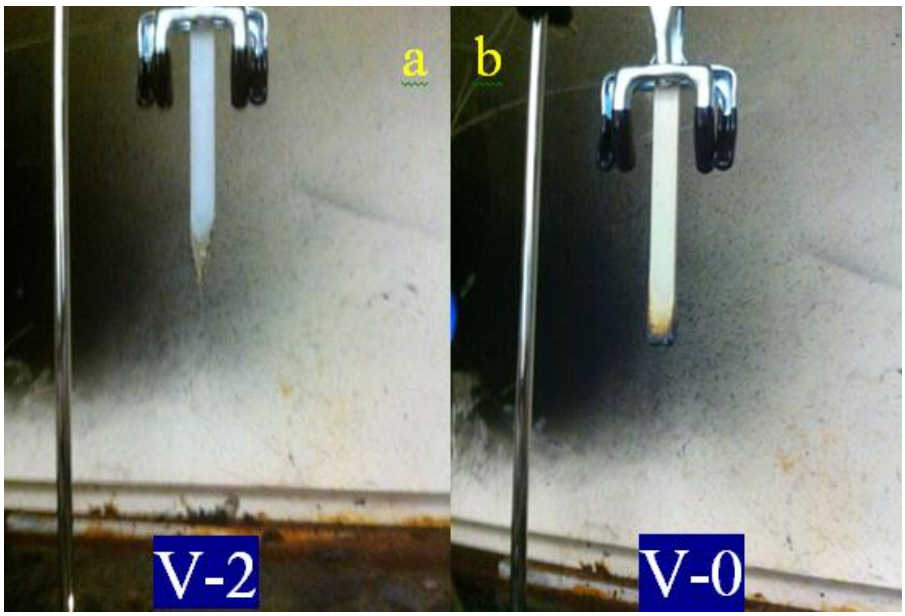

Figure 13. Samples #1 and #6 after UL 94 test.

2.4.5 Char Characterization of Twin Screw Extruded Bulk Materials

SEM analysis was performed on the cross section of charred samples of FR-NC-PA6 after the UL 94 test as shown in Figure 14 and Figure 15. It can be observed that the combination of nanoclays and FR additives reduced the flammability by forming an insulating char structure on the surface of the polymer nanocomposite. The additives effectively assembled into a heat shield, preventing the polymer from burning beneath the charred surface. EDX spectra of the char surface (Figure 16) shows obvious peaks of carbon, oxygen, sodium, aluminum, silicon and phosphorus, confirming the char shield

was mainly composed of carbonaceous char (C, O), nanoclay (Na, Al, Si, O) and FR (O, P).

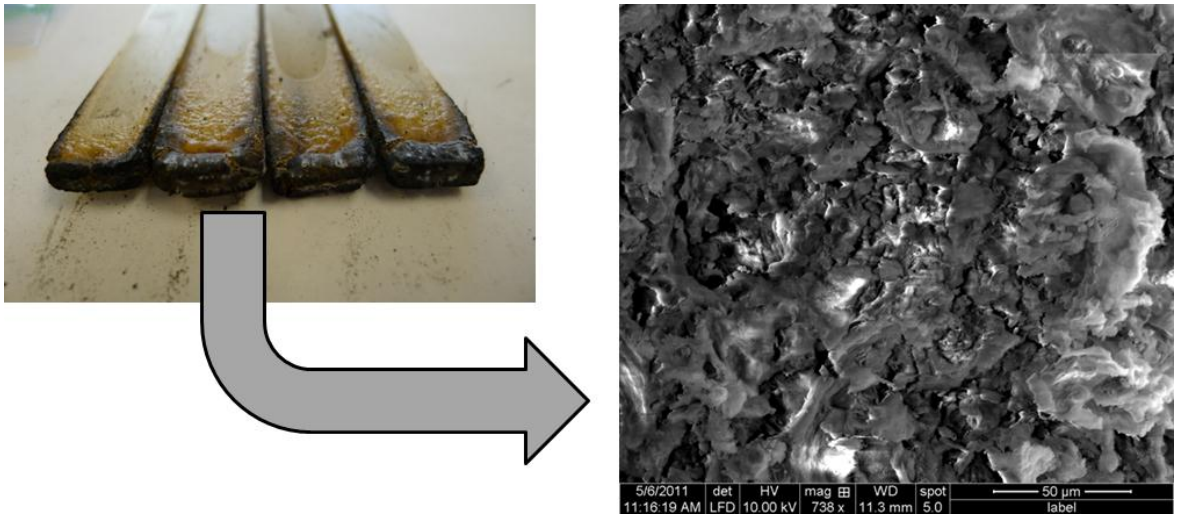

Figure 14. SEM image on char surface of #6.

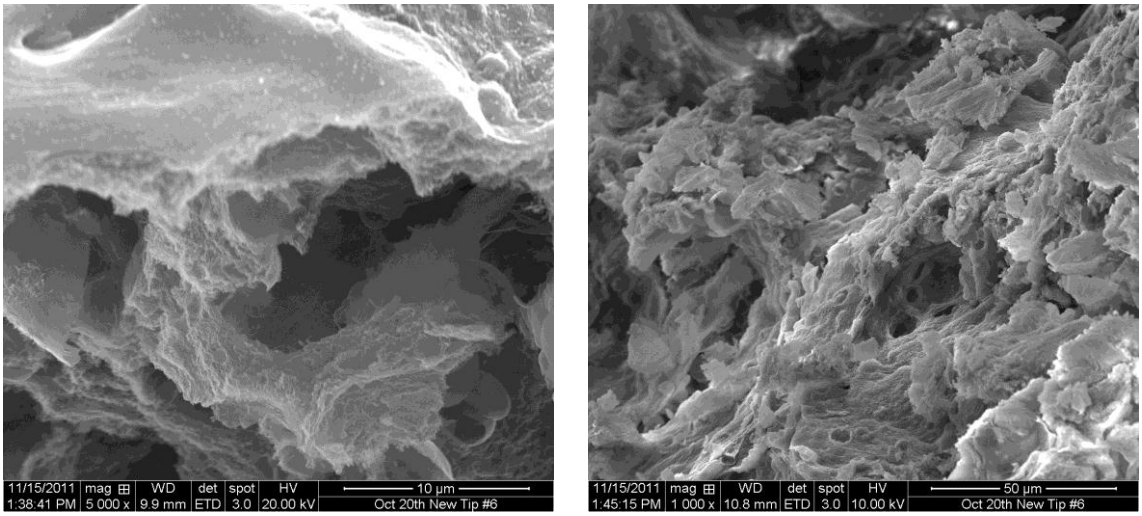

Figure 15. SEM image of char fracture surface of #6.

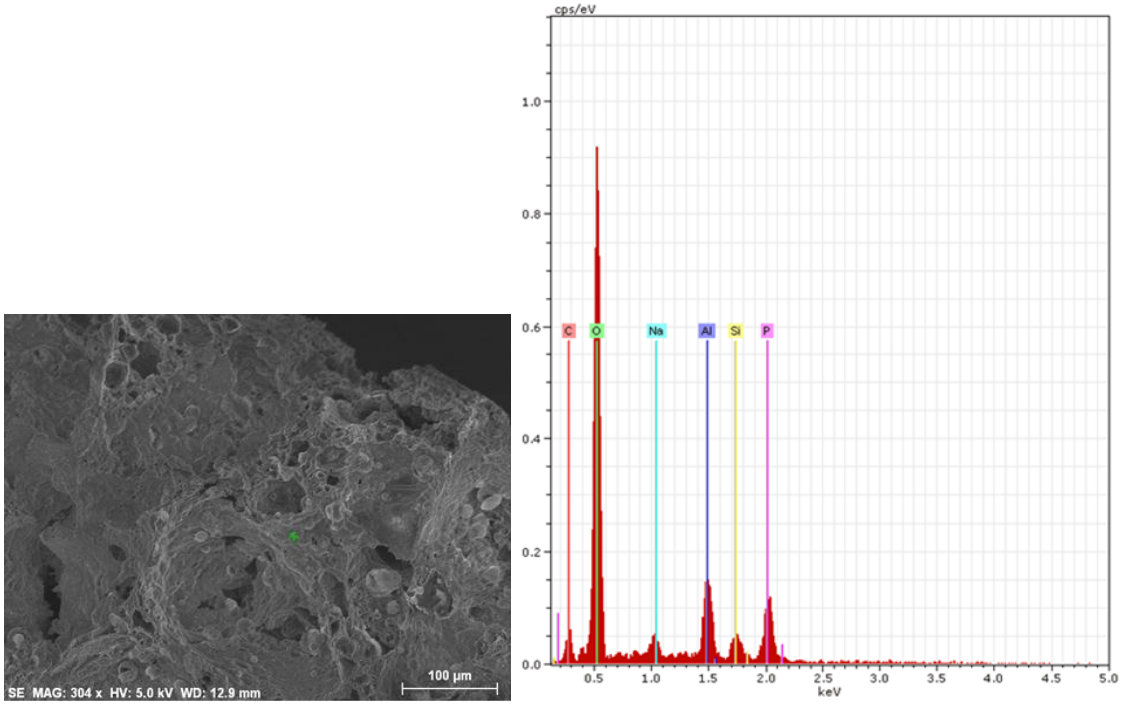

Figure 16. SEM and EDX of char surface of #6.

2.4.6 Characterization of Combustion Properties by MCC

A comparative study was first conducted to identify if there is any difference in heat release rate between bulk form material and electrospun samples with the same composition. As shown in Figure 17, the "Temperature" versus "Heat release rate" curve of samples #1 appears to be identical; this indicates that electrospinning did not impact MCC combustion properties of neat PA6. Similar results were also found on other composite samples, such as #7 shown in Figure 18. Thus we assume this test is form or shape independent, and will use suffix "B" to indicate bulk form samples and "F" to indicate fiber form samples.

Heat release capacity is a true material property which only depends on thermodynamic state values and independent of sample size or heating rate [42]. Heat

release capacity (η c) results for the samples tested by the MCC are shown in Figure 19. It shows mean plots with 95% confidence intervals. Again, the compression-molded film and electrospun fibers show similar results for the neat PA6. The results of the FR-NC-PA6 formulations appear to be dependent on the weight percent of the additives. A compression-molded film of the nanocomposite formulation containing 5wt% NC and 20wt% FR particles (#6) resulted in a 26% reduction of η c. The amount of fillers in the electrospun formulations had to be decreased in order to facilitate the collection of continuous fibers. Figure 19 shows that the electrospun formulation with lower amounts of MMT and FR intumescent additives (2.5wt% and 10wt%, respectively), also achieves a significant decrease in η c. However, the electrospun formulation containing only 1.25wt% MMT and 5wt% FR has a similar heat release capacity as neat PA6, indicating that this level of additives would not be sufficient to achieve flame retardancy.

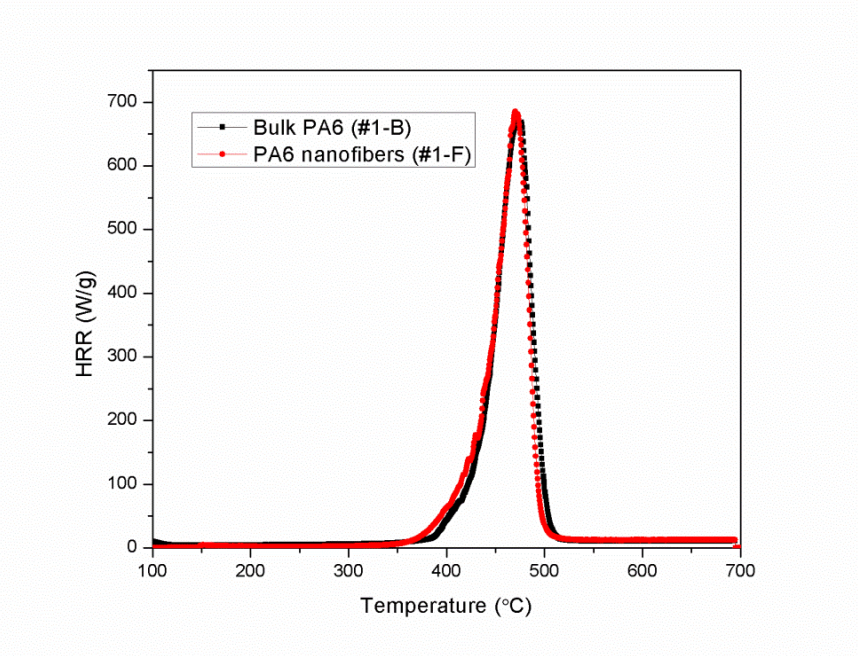

Figure 17. Comparison of MCC curves of neat PA6 (#1) in different forms.

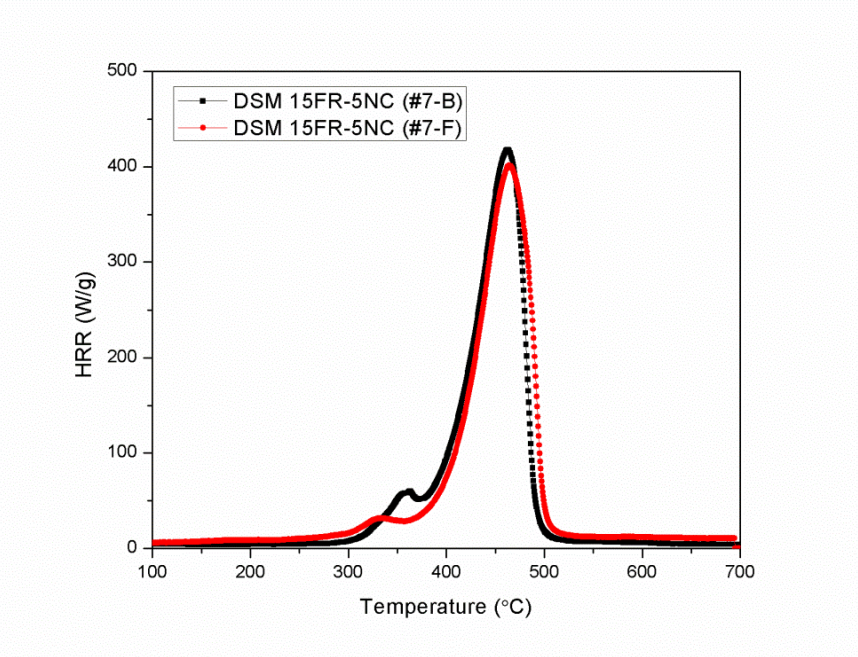

Figure 18. Comparison of MCC curves of DSM 15FR-5NC (#7) in different forms.

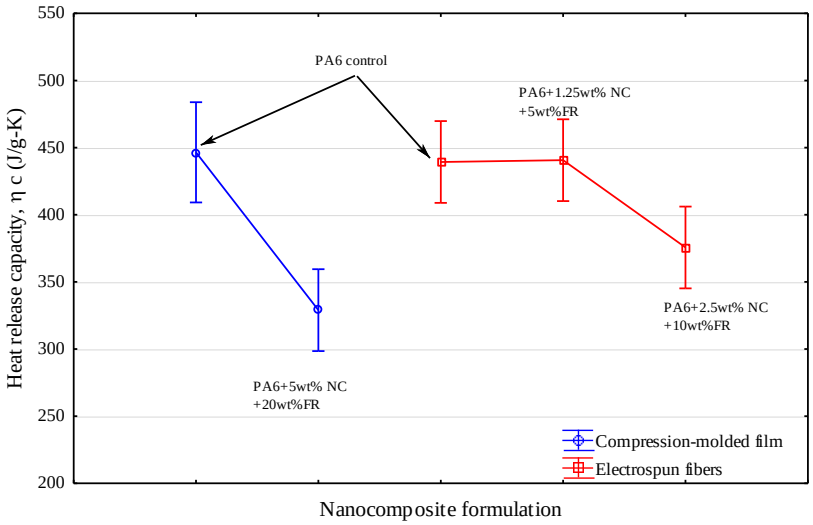

Figure 19. Heat release capacity, η_c (J/g-k) for various FR-NC-PA6 formulations in both compression-molded film and electrospun fiber forms.

For twin extruded bulk materials (Figure 20), the peak heat release rate of formulation #6-B decreased from 685.0 to 328.5 (more than 50%) with 20wt% FR and

5wt% NC. This confirmed the effective enhancement in flame retardancy that was found in UL 94 test. For electrospun fibers by solution blending (Figure 21), it was found that FR wt% played a major role in determining peak heat release rate. In this case, formulations #2 and #3 both have a peak HRR around 450 W/g, formulations #4 and #5 have a peak HRR close to 350 W/g, which is 20W/g higher than that of bulk twin-screw extruded sample #6 containing 20wt% of FR and 5wt% of NC.

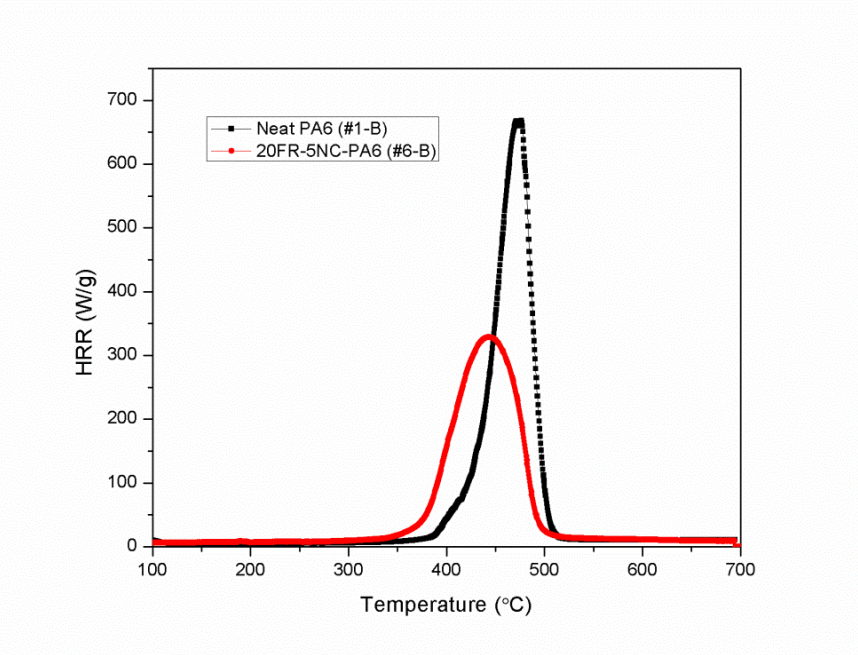

Figure 20. Twin screw extruded bulk samples.

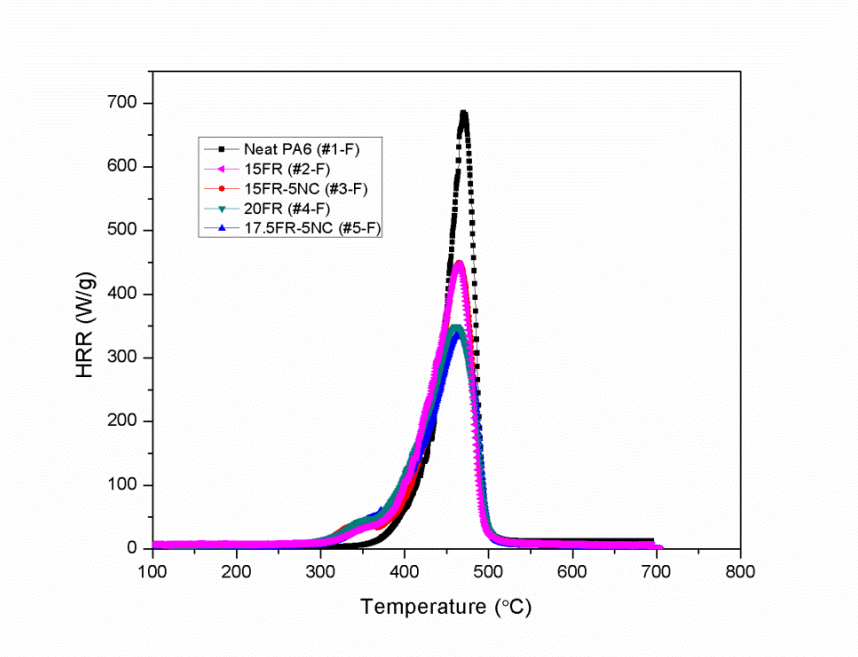

Figure 21. Comparison between solution-blended nanocomposite fibers.

For twin-screw extruded samples (Figure 22), low peak heat release rate was observed, indicating the synergistic effect of clay and flame retardant are found in sample #6. However, with 20wt% FR and 5wt% NC loading, the temperature at which peak Heat Release Rate (HRR) is reached decreased by roughly 20°C.

Figure 23 summarizes the heat release capacity of all the samples in this study. Each error bar is calculated by 3 repetitions. From the summary, it is obvious that neat nylon 6 has the highest HR capacity with an average value at 658 J/g-K. For solution blended samples from #2 to #5, the HR capacity is largely dependent on the concentration of FR rather than NC. For high shear pre-mixed samples, formulation #6 has the lowest HR capacity while for #7 and #8 FR concentration also plays a dominant role in determining HR capacity.

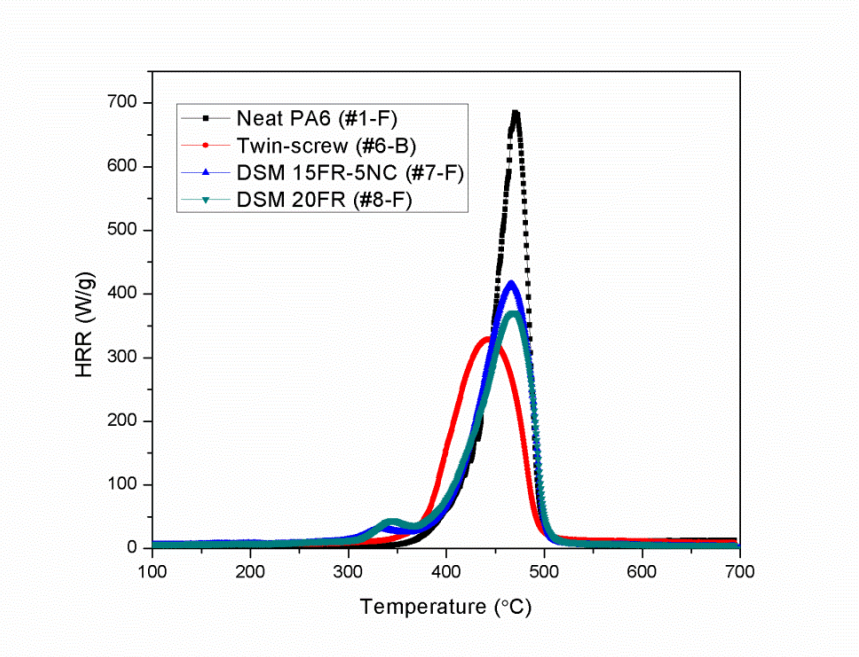

Figure 22. Comparison between high shear pre-mixed samples.

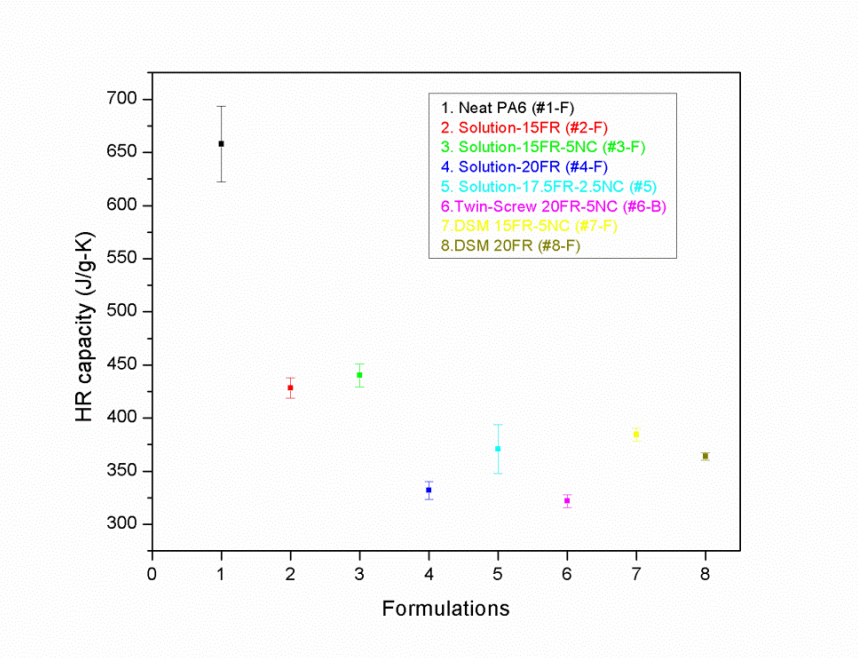

Figure 23. Heat release capacity of all formulations.

2.4.7 Electrospun fiber morphologies

All formulations made by high shear pre-mixing were homogeneously blended in formic acid. No precipitation was observed even after storage for several days, indicating a good dispersion of FR and NC. However, for solution-blended solutions depositions were observed after being stored for several days. SEM images of samples electrospun from the 30% neat nylon 6 solution at 27kV (Figure 24) show fibers with smooth surfaces and uniform diameter around 200 nm. Meanwhile, when higher voltage was applied (35kV), flat-sheet or ribbon-shaped fibers with diameters as large as 1 μm were observed. Fong et al. also reported ribbon-shaped fibers of electrospun nylon-6/hexafluoroisopropanol (HFIP) [43]. The authors stated that rapid solvent removal from the surface of the jet presumably forms a skin, reducing subsequent solvent evaporation. This skin may cause the formation of hollow tubes, which subsequently collapse to form ribbons. Ribbon-shaped electrospun fibers and branched fibers have been reported for a number of different kinds of polymers and solvents [44, 45].

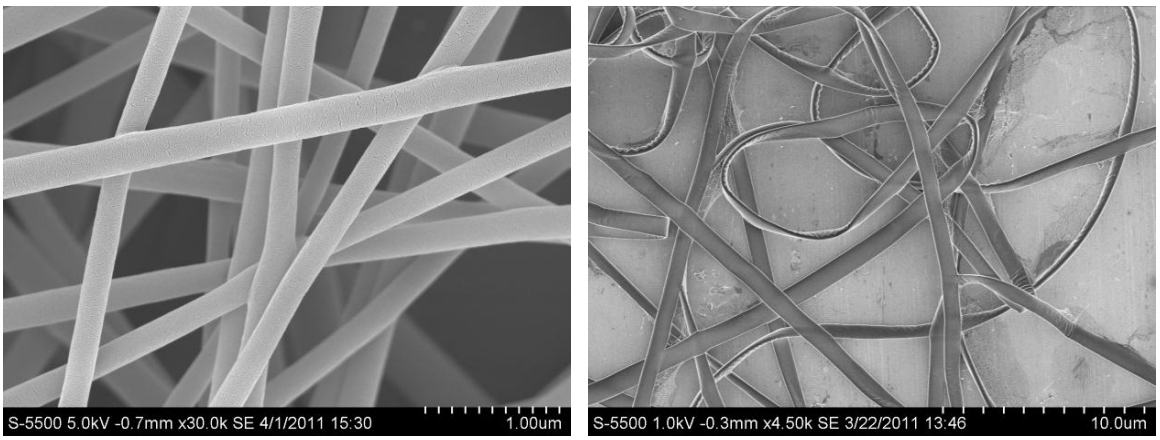

Figure 24. SEM images of electrospun fibers of formulation #1.

Fibers with relatively rough surface structures were electrospun from the formulation #6 solution at the same concentration (Figure 25). However, the spinning

process was not continuous; solution at the needle point splashed from time to time when voltage was applied. This may be due to the addition of clay and intumescent FR that increased the Raleigh instability of the solution [46] and reduced its electrospinnability as discussed in 2.2.3.3. The protrusions distributed along the fiber axis are expected to be exfoliated clay platelets. It was also noticed that some fine fibrous web structures with diameters as small as a few nanometers were formed between larger fibers (Figure 25).

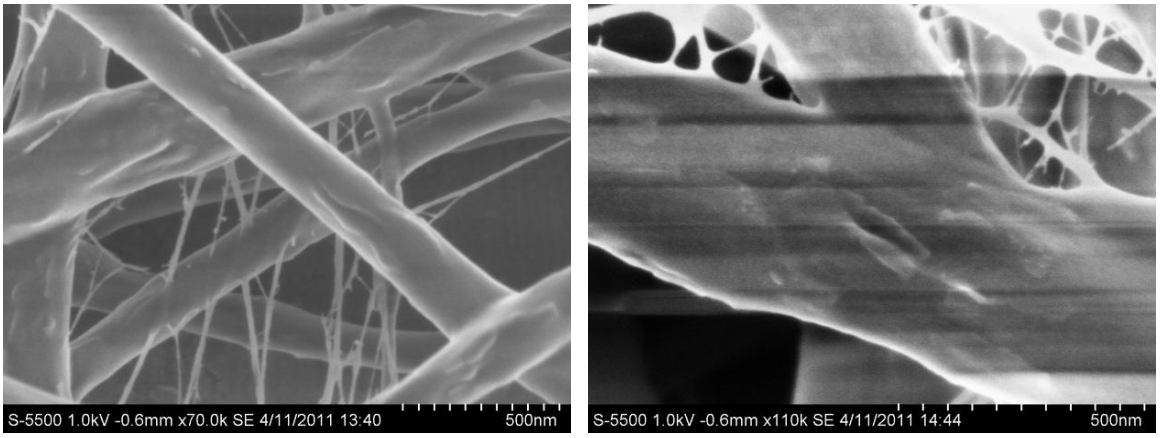

Figure 25. SEM image of electrospun fibers of formulation #6.

In order to improve the electrospinnability, formulations #1 and #6 were blended in formic at two different ratios; 3:1 and 1:1. The diameter of the 3:1 mixed fibers which contain 1.25wt% clay appeared to be very uniform at about 200nm (Figure 26). The surfaces of these fibers are relatively smooth with slight textures along the fiber axis. The protruding linear textures may be exfoliated clay platelets. Further studies are needed to confirm this assumption.

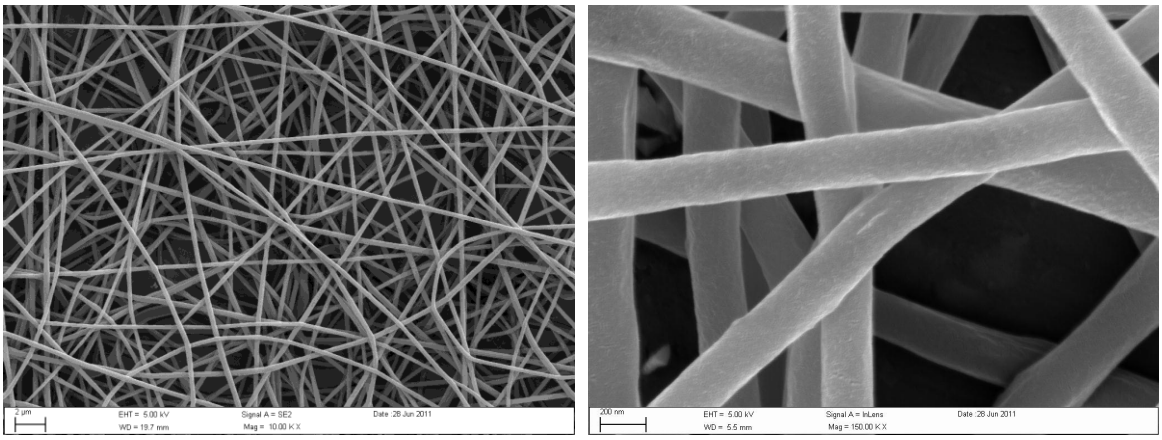

Figure 26. SEM image of electrospun fibers of the blend #1/#6 at ratio of 3:1.

It is obvious that with the addition of fillers in the 3:1 mixed formulation, the fiber surface (shown in Figure 27 and Figure 28) appeared to have more textures on the fiber surface. However, the diameter of these fibers (300-400 nm) does not appear to be very uniform; some helical or spiral fibers are observed from Figure 28. The increase of fiber diameter may be caused by the increased viscosity and lowered conductivity of the spinning solution due to the addition of clay and FR additives. The increased viscosity may also be the reason for the formation of beads on the string structure as observed in Figure 27.

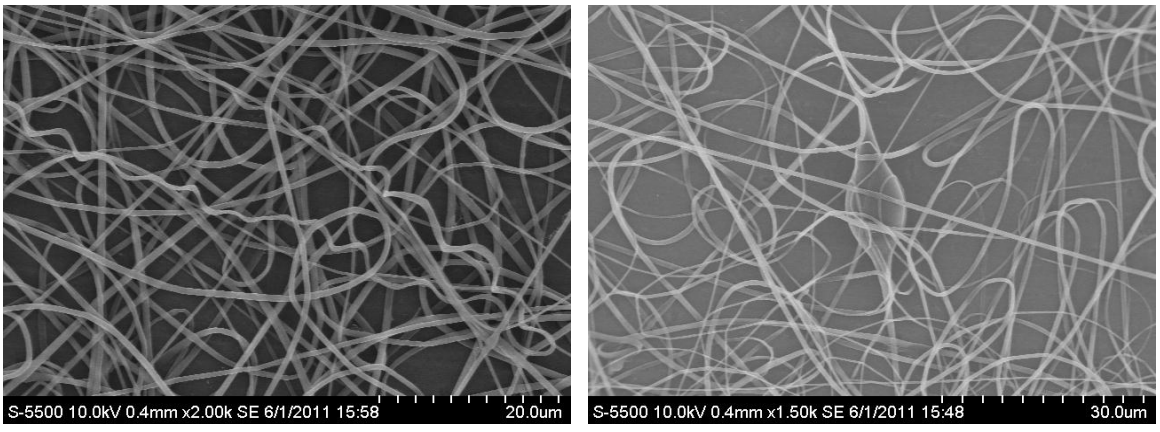

Figure 27. SEM image of electrospun fibers of #1/#6 at ratio of 1:1 (a).

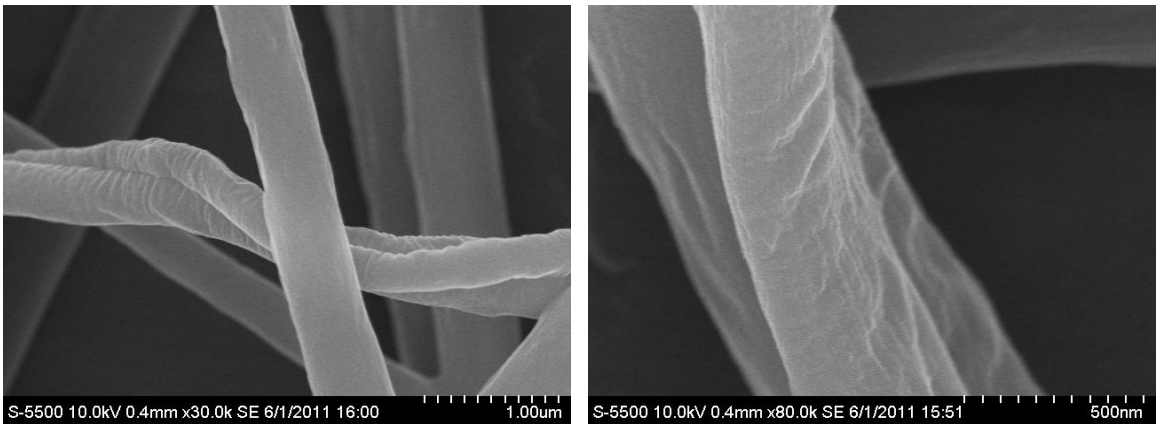

Figure 28. SEM image of electrospun fibers of #1/#6 at ration of 1:1 (b).

All solution-blended formulations were successfully electrospun. Figure 29 shows SEM images of electrospun sample #2, which only contains 15wt% of FR and 85wt% of PA6. The overall fiber diameter appears uniform at roughly 100nm with some fine fibrous protrusions forming a web-like structure. It is noticed that there are some particles embedded within the fiber mats, which indicated that the FR particles are not small enough to be incorporated in the fibers, but will be trapped in between fiber layers. Samples #3 and #4 have similar structures as #2. From Figure 30 and Figure 31, it can be observed that fibers at intersections are welded with other fibers attached to them. With higher FR loading as shown in Figure 32, it is possible to get larger FR particles at about 1 micron embedded in the fiber web. This indicates that FR additives may re-agglomerate to form larger sized particles.

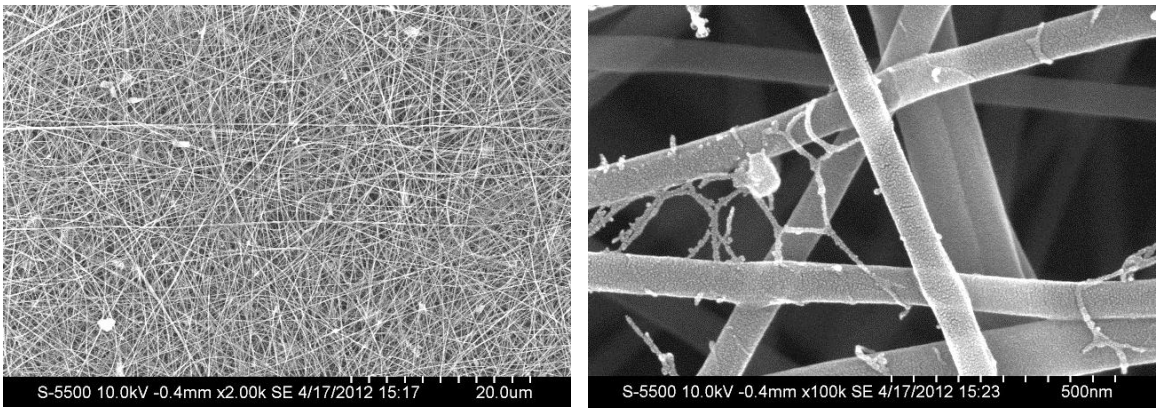

Figure 29. SEM of electrospun fibers of #2 (15FR).

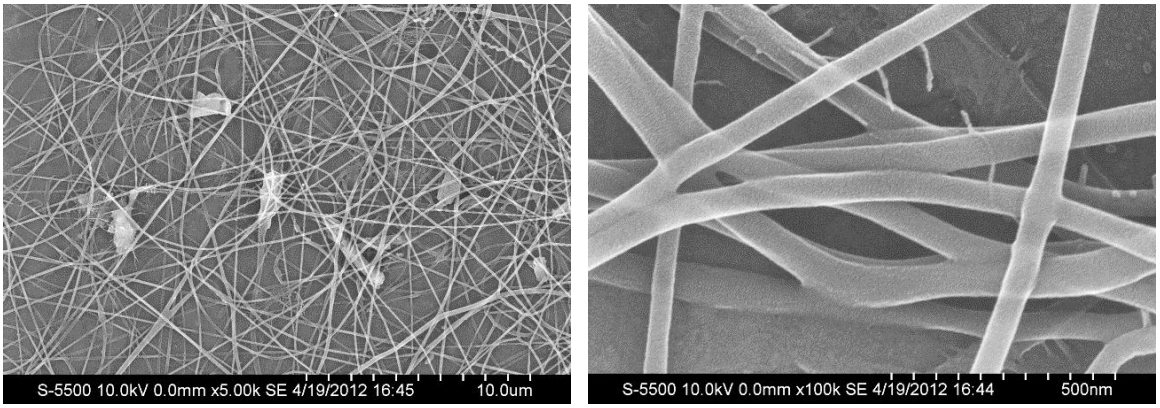

Figure 30. SEM of electrospun fibers of #3 (15FR-5NC).

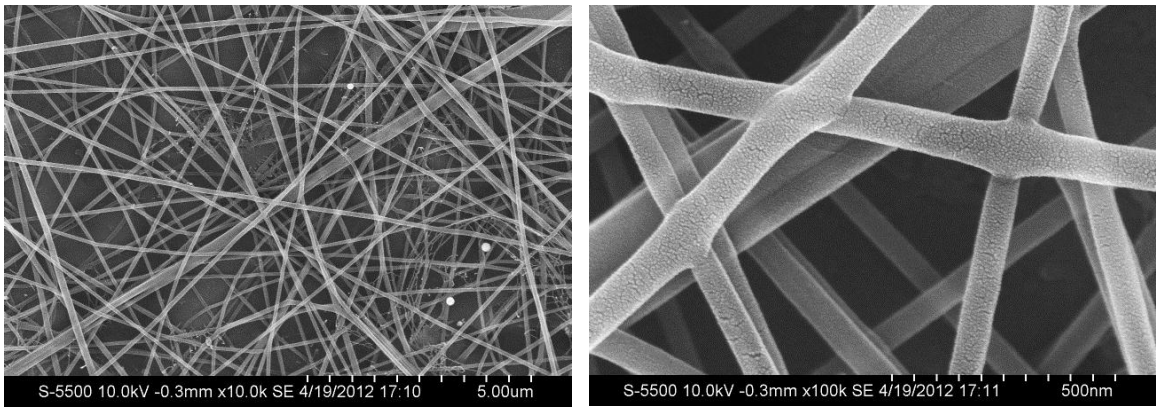

Figure 31. SEM of electrospun fibers of #4 (20FR).

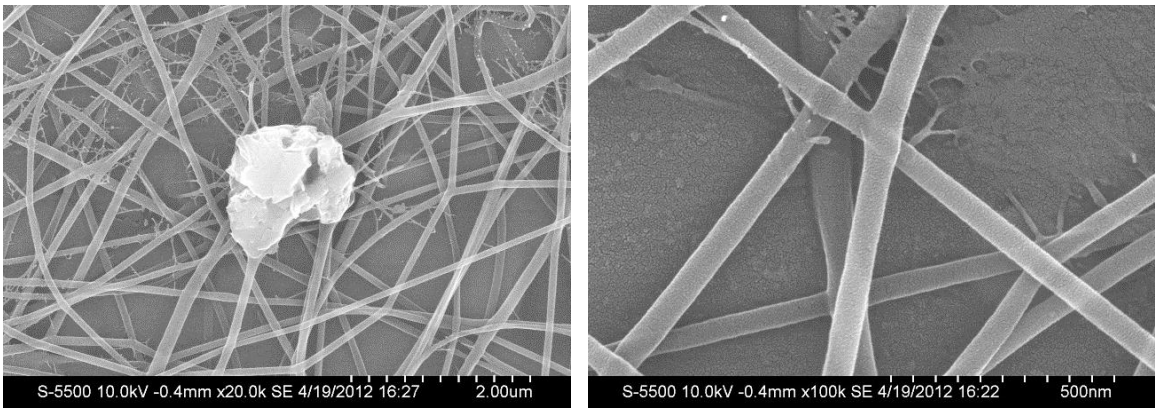

Figure 32. SEM of electrospun fibers of #5 (17.5FR-2.5NC).

Samples that are premixed using DSM micro-compounder were successfully electrospun with no observable instability during the entire process. Fibers containing 15wt% FR and 5wt% NC are shown in Figure 33. From the image on the left, it can be seen that some FR particles are embedded in the fiber mat. This is similar to what has been observed in Figure 30. The average fiber diameter is uniform at around 100nm from the image on the right. Some fine texture or protrusions along the fiber axis can be observed which could be exfoliated clay platelets. For sample #8 which contains 20wt% FR, the fiber structure shows no significant difference from #7 except that the surface is texture free and more fine fibrous webs were observed.

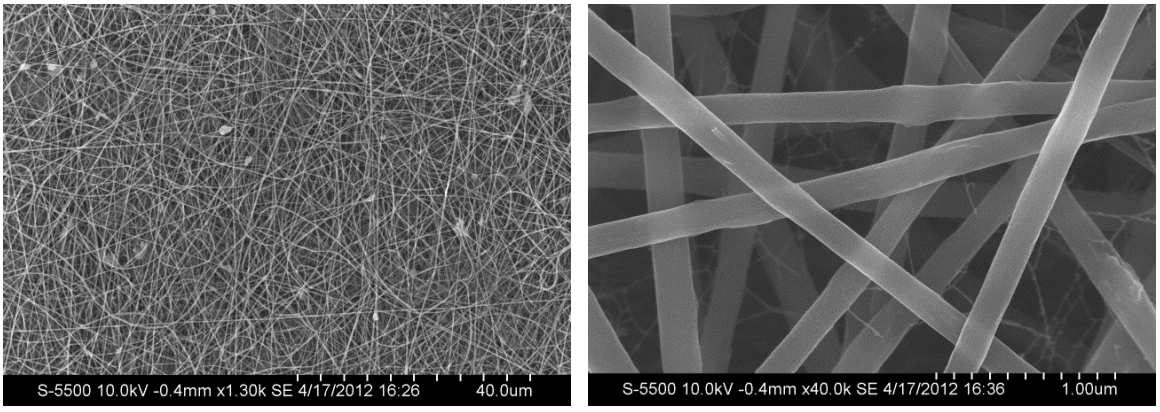

Figure 33. SEM images of electrospun formulation #7.

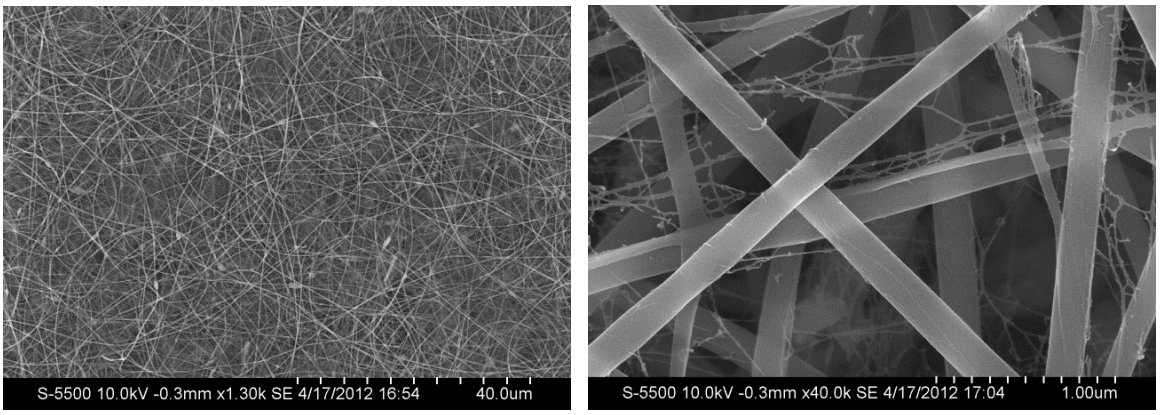

Figure 34. SEM image of electrospun #8 by solution blending.

2.5 SUMMARY

In summary, electrospun flame retardant nanocomposite fibers were synthesized and characterized. Two methods of mixing FR and NC additives into nylon 6 polymer were explored. With 20wt% FR and 5wt% NC, extrusion molded bulk sample #6 have increased Young's modulus significantly from 1.436 to 2.685 GPa compared to neat PA6. However, the ultimate tensile strength dropped from 59.3 to 49.4 MPa, and the elongation at break declined dramatically from 230% to 3.1%. Samples with FR and NC passed UL 94 V-0 while neat sample was only rated as V-2. Although TGA analysis indicates there is a lower starting temperature of decomposition for composite sample #6, MCC results on both bulk and fiber materials proved that the FR and NC helped to decrease heat release rate during combustion. Moreover, it seems FR played a major role in reducing flammability of the material. SEM analysis was performed on all the electrospun fibers to reveal a detailed structure of the material. It was found that FR additives even after wet milling are still too large to be incorporated in these ultra-thin fibers with typical diameter ranging from 100 to 200 nm. Moreover, high concentrations of FR and NC will render poor electrospinnability because of insufficient elasticity of the electrospinning fluid.

Chapter 3 Superhydrophobic Modification of Nylon 6 Nanocomposite Fibers

3.1 Introduction to Superhydrophobicity

Surfaces with water contact angle (WCA) higher than 150 degrees are called superhydrophobic surfaces. Such surfaces have attracted extensive research interests during the last decades owing to their potential to be utilized in many applications, such as self-cleaning and protective clothing, enhanced corrosion-resistant surfaces and more recently in the energy transition related field such as battery and fuel cell application [47-51]. Figure 35 is an illustration of water contact angle. Inspired by nature's plants and animals, bionic studies on biological superhydrophobic surfaces like lotus leaf and water strider leg showed that superhydrophobic surfaces can be achieved by a combination of low surface energy materials and hierarchical surface roughness in the micrometer or nanometer scale [48, 49, 52, 53]. These surfaces usually have very low contact angle hysteresis (<5-10 degrees) and low threshold sliding angle [54-56]. When a liquid is dropped on the surface, a "re-entrant" geometry will be formed in which liquid droplets on the surface can be retained in the Cassie-Baxter state; air pockets will be trapped underneath the liquid, therefore reducing the solid-liquid interface[57]. However, extremely low surface energy is not necessary to achieve superhydrophobic surfaces; instead, the ability to control the surface morphology on the micron and nanometer scales is key [49, 58].

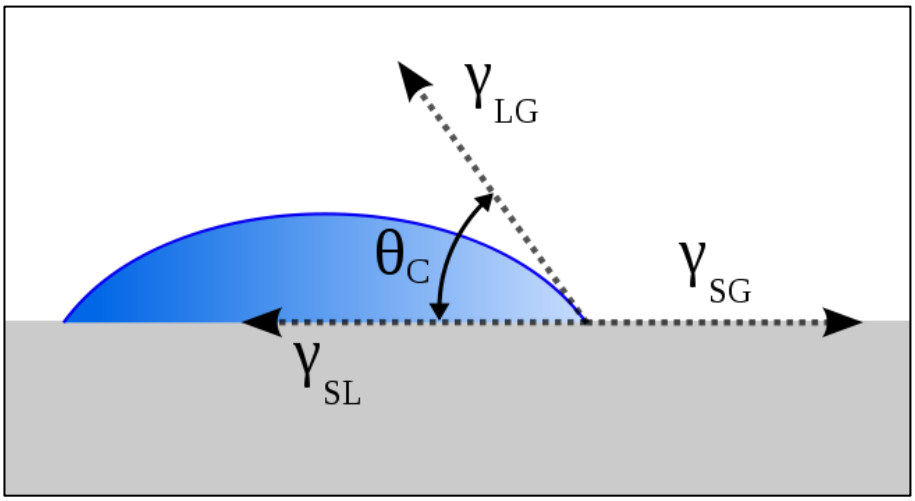

Figure 35. Illustration of water contact angle.

Knowing the principle behind superhydrophobicity [57, 59, 60] have led to the development of numerous artificial superhydrophobic surfaces with hierarchical roughness prepared by various methods [61]. For example, Shirtcliffe [62] et al. grew copper pillars onto flat copper by electrodeposition; the resultant surface showed a water contact angle as high as 165°. Wang et al. fabricated superhydrophobic surfaces made of T-shaped micro-pillars with various densities and sizes coated with diamond-like carbon on a silicon Si-wafer [63]. Ming et al. synthesized superhydrophobic films containing raspberry-like silica particles with water contact angle as high as 165°[64]. Hsu et al. recently developed artificial hairy surfaces with nearly perfect hydrophobicity and indistinguishable contact angle hysteresis using pressurized membrane casting [65]. Wang et al. fabricated super hydrophobic surfaces by depositing fluoropolymer transparent thin films using one-step vacuum evaporation method [65].

Among different types of surface structures, fibrous materials have drawn interest due to their wide range of applications [66-68]. For example, Tuteja et al. created rough fluorodecyl POSS-PMMA surfaces by electrospinning. The resultant surfaces exhibited

WCA ranging from 130° to 160° with different mass fractions of flurodecyl POSS, while the WCA of spin-coated films of PMMA and fluorodecyl POSS film were no larger than 125° [49]. In order to get hierarchically roughened surfaces, Ma et al. synthesized superhydrophobic electrospun nylon 6 fibers by using two different approaches, i.e., fabrication of porous fiber morphology and fiber coating with silica nanoparticles by means of layer-by-layer (LBL) assembly technique [69]. The resultant WCA were 163° and 168°, respectively. Chiou et al. aligned polyaniline nanofibers using chemical oxidative polymerization and used CF4 plasma treatment to create superhydrophobic surfaces with a contact angle of 175° [70].

Plasma treatment has proven to be a simple and effective tool for surface modification without affecting the desired bulk properties of a material, such as strength, and toughness [71-73]. The use of C_xF_y plasma treatments to introduce fluorine groups on polymer surface is an effective way to lower surface adhesiveness, surface energy and coefficient of friction, and form super-hydrophobic surfaces [74].

The goal of this study is to explore a new approach to achieve superhydrophobicity. By adding nanoclay into polymer nanofibers, a second level of roughness on the fiber surface is expected. Previous research [30] has shown that montmorillonite nanoclay could be well dispersed into nylon 6. Unlike previous methods that only modify the fiber surface with nanoparticles or synthesis porous fiber structures; in this study, it is the first time to combine nylon 6/clay nanocomposite fibers with plasma treatment to produce a super hydrophobic surface. Compared to alternative methods plasma treated polymer-clay nanocomposite fibers has many advantages: (a) a simple two-step process for the conformal coating of polymer fiber with hydrophobic material; (b) internally constructed hierarchical roughness; and (c) a large variety of available materials for processing.

3.2 EXPERIMENTAL METHODS

3.2.1 Materials & Experimental Design

The same grade of nylon 6 and nanoclay were used in this section. Mixtures of nylon6 and nanoclay were pre-mixed using twin screw extrusion. Exfoliated nanoclay was homogenously distributed within nylon 6 solution for electrospinning. The electrospun nanocomposite fiber with wrinkled texture could be considered as a second level of roughness for superhydrophobic materials. Surface modification was achieved by inductively coupled plasma (ICP) treatment for both neat electrospun nylon 6 fiber mats and nanocomposite fiber mats. In order to find the effect of clay concentration on the surface roughness, 4 different loadings of clay were incorporated into nylon 6, namely 0wt%, 1.25wt%, 2.5wt%, and 5wt%. Each formulation was then treated by ICP for 4 different durations: 0s, 30s, 1min and 5min. It is expected that both of the samples will have a WCA larger than 150°; nanocomposites fibers mats will exhibit larger WCA than pure nylon 6 fibers.

3.2.2 Fabrication

Fibers containing different concentrations of nanoclay were electrospun using same apparatus as described in Chapter 1. In order to decease the surface energy and improve the surface roughness, plasma enhanced chemical vapor deposition (PECVD) is applied as a simple process used to deposit thin films from a gas state (vapor) to a solid state [72]. Plasma Lab 80+ (Oxford Instruments) from Texas Material Institute (TMI) was used in this study. Samples were first vacuumed to 5E-4 Pa and cooled to 15°C;

C4F8 was introduced into the chamber at a flow rate of 100 sccm. The plasma generated has a RF power of 150W, and ICP Power is also 150W.

3.2.3 Characterization

Surface hydrophobicity of both treated and untreated samples were evaluated by static contact angle measurement using a VCA Optima® system (AST Products Inc.). The values reported in the result correspond to five randomly selected points on the tested surface. SEM (Hitachi S-5500) was used to observe the difference in fiber surface morphology before and after the plasma treatment. All samples were characterized without surface coating and low beam energy was used. Surface topography was characterized by tapping mode Atomic Force Microscopy (AFM) (Agilent 5500) from Texas Materials Institute (TMI). 3D image reconstruction from raw data was processed by Gwyddion (developed by Czech Metrology Institute).

3.3 RESULTS AND DISCUSSIONS

3.3.1 Static Contact Angle Test Results

Samples without plasma treatment show different contact angles as illustrated in Figure 36. For neat PA6 the initial contact angle is 42° and the contact angle keeps decreasing over time. Interestingly, for samples with 1.25wt% and 2.5wt% clay, water droplets spread over the fiber mat immediately after touching the surface. For samples with 5wt% clay loading, even the untreated sample shows a contact angle of 140°, substantially higher than neat and low clay loading samples. This could be due to the "barrier effect" of nanoclay [75]. For the untreated sample, the water droplet keeps its

form but appears attached to the surface, which means it will have a high roll off angle. Further characterizations on dynamic roll-off tests are needed to quantify this phenomenon.

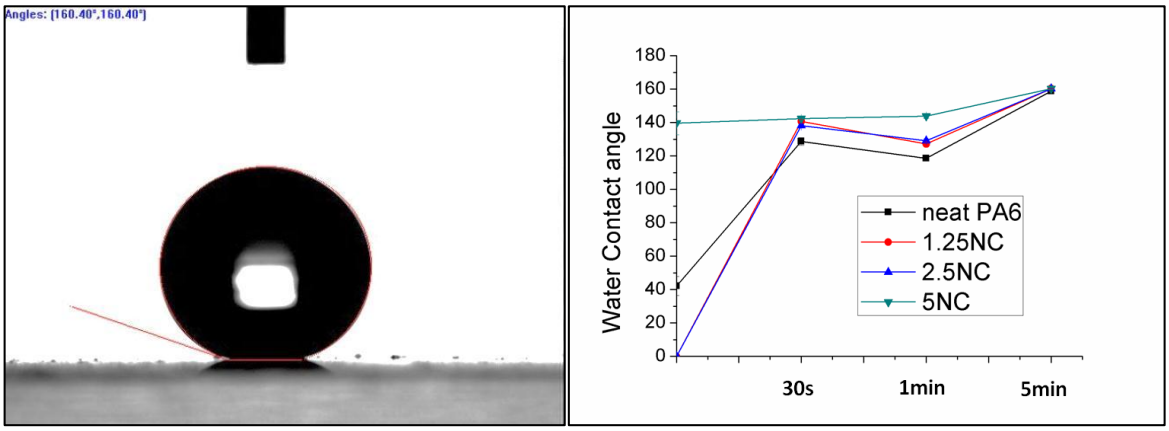

Figure 36. Static water contact angle test.

It is shown that 5min of plasma treatment gives all the samples almost the same contact angle at 160° (Figure 36); this might be because all the samples are over treated, which means that the ablation effect creates extra roughness by destroying some of the fiber structures.

3.3.2 SEM Results

Neat nylon 6 fibers (Figure 37) exhibited a ribbon shaped structure with lateral dimension of about 3 μm and thickness of about 200nm. After 5min of plasma treatment, some of the fibers were partially etched away. The remaining fibers have a fine roughened surface.

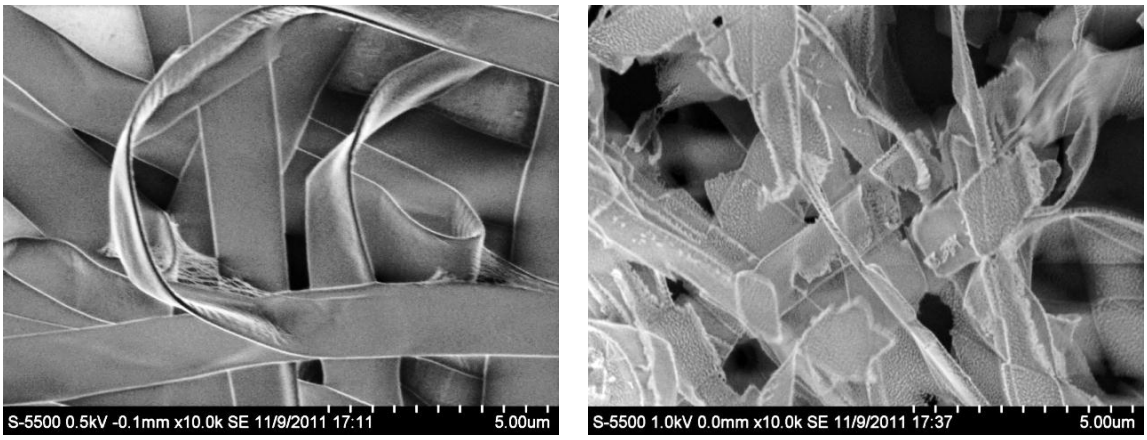

Figure 37. SEM image of electrospun PA6 fibers before (#1) and after plasma treatment (#13).

Fibers with 5wt% of clay have a circular round shape (Figure 38), with a diameter of about 500nm. Plasma treated fibers show a roughened surface with some white dots on top.

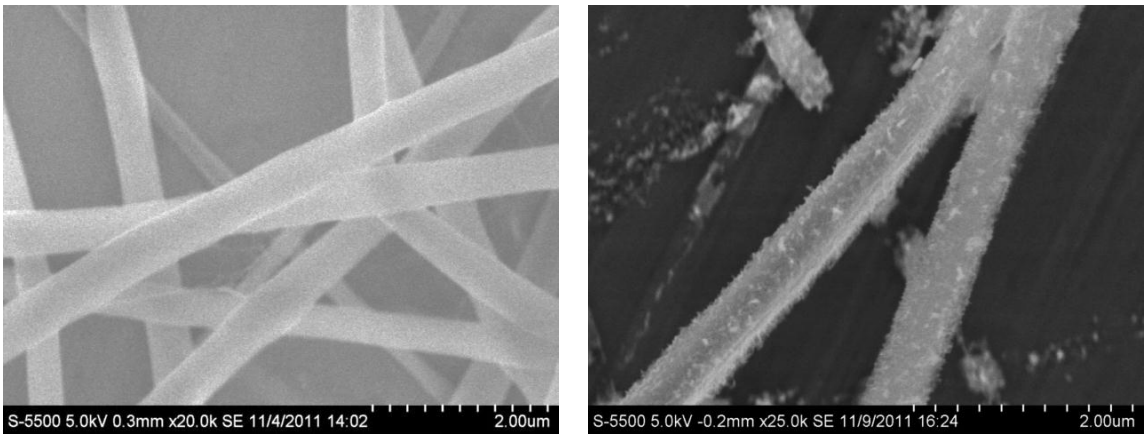

Figure 38. SEM image of electrospun 5NC-PA6 fibers before (#4) and after (#16) plasma treatment.

3.3.3 AFM Results

AFM images (Figure 39 and Figure 40) show that both neat PA6 and 5NC have a very smooth surface before plasma treatment. Although 5NC have a flat smooth under AFM, it still have WCA of 140°, this could be due to the barrier effect of clay as described in 3.3.1. Surfaces of neat nylon6 treated with 5 min plasma have a rough surface with maximum height of 80nm. The 5wt% clay incorporated fibers have surface with protrusion height as high as 340nm.

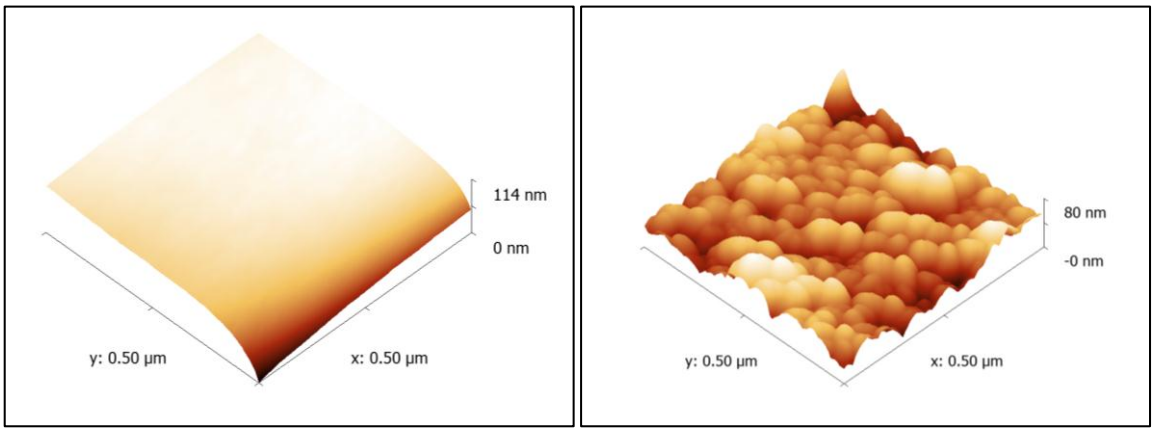

Figure 39. AFM image of electrospun PA6 fibers before (#1) and after (#13) 5min plasma treatment.

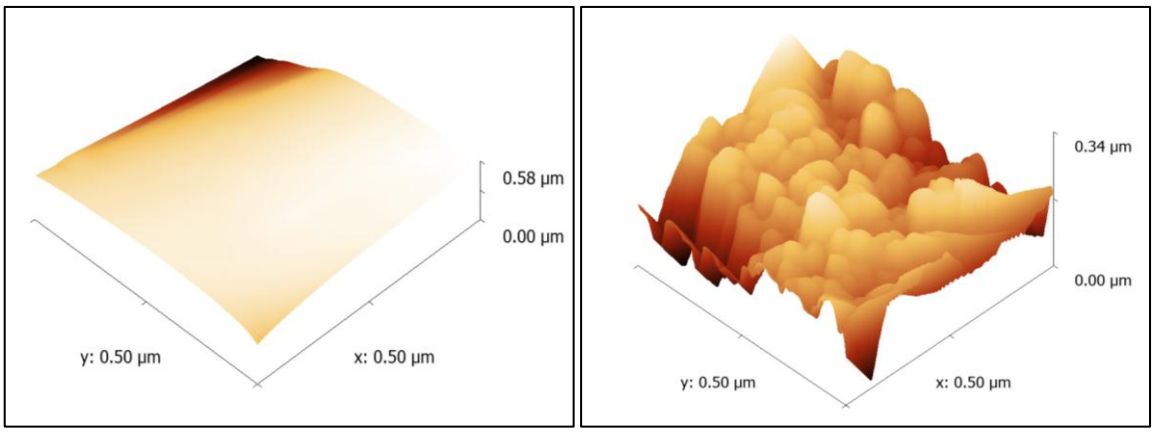

Figure 40. AFM image of electrospun 5NC fibers before (#4) and after (#16) 5min plasma treatment.

3.4 SUMMARY

In this section, superhydrophobic surfaces were successfully created by a combination of internal and external modification of neat nylon 6 based on electrospinning. While the internal modification was achieved by adding nanoclay into the polymer solution, external modification was done by plasma deposition of low surface energy fluorine materials. Static water contact angle analysis indicates that 5min of plasma duration will produce the highest hydrophobicity with water contact angle at 160 despite the clay concentration. However, SEM image reveals that such long plasma exposure partially destroyed the structural integrity of the fiber mats. AFM characterization confirmed that when the etching effect of plasma treatment was dominant, a higher roughness would be expected. Nevertheless, other properties, such as mechanical property should also be taken into consideration to guarantee a decent durability of the materials in practical scenarios.

Chapter 4 Conclusion and Future Work

In this study, two major areas of interest were explored. In the first part, flame retardant electrospun nanocomposite fibers with various concentrations of FR and NC were successfully synthesized. Two methods were selected for dispersing FR and NC to make electrospinning fluids, namely "high shear pre-mixing" and "solution blending". Samples with 20wt% FR and 5wt% NC passed UL-94 V-0 with no dripping, while neat nylon 6 sample was only rated as V-2. Although TGA analysis indicate there is an lower starting temperature of decomposition for the composite samples, MCC results on both bulk and fiber forms of these composite materials proved that the addition of FR and NC fillers could effectively decrease heat release rate during combustion. In general, FR additives have a more dominant effect on flame retardant properties while the addition of NC will produce more char residue after combustion. This char residue will act as a thermal shield to protect the inner layers of the material. It was also found that with high loadings of NC and FR, elongation at break will decrease by more than 85%, which is not desirable for making textile fibers. SEM images on all the electrospun fibers revealed that FR additives even after wet milling were still too large to be incorporated in these ultra-thin fibers whose typical diameter ranges from 100 to 200 nm. Moreover, high concentrations of FR and NC will render poor electrospinnability because of insufficient elasticity of the fluid.

Such flame retardant electrospun nylon 6 fibers could have potential to be used as a functional layer in protective clothing system or high efficiency filter membranes where flame retardant property is also needed. In the future, more characterization methods on mechanical properties of electrospun fibers should be developed to identify if there is any difference in terms of elongation at break. On the other hand, other functional nanofillers,

such as Polyhedral oligomeric silsesquioxane (POSS) could also be analyzed as an alternative to nanoclay. POSS may also help to improve elongation at break.

For the superhydrophobic function, nanoclay particles incorporated nylon 6 were successfully electrospun into nanofibers with typical diameter between 500-600nm. The addition of clay tended to facilitate forming circular shaped fibers while neat nylon 6 under the same conditions formed ribbon-shaped fibers. 5wt% of clay even without plasma treatment greatly improved the water contact angle due to the barrier effect of nanoclay. Furthermore, plasma treatment could effectively modify surface energy of the fibers as well as their roughness. When samples are overexposed to the plasma, fiber structure will be partially etched. Clay-loaded samples have a better resistance to etching than neat nylon 6. For future work, one may consider optimizing plasma treatment time, in order to create roughened fiber surface without compromising its structural integrity. Finding out the influence of clay loading and fiber diameter on hydrophobicity will also be of interest.

References

[1] Navigating Flame Retardancy Regulations in the United States. http://www.sewwhatinc.com/fr_in_US.php: Sew What? Inc.; 2012.
[2] Feynman R. There's plenty of room at the bottom. Engineering and Sciecne. 1959:22-36.
[3] NSF, Web, site. Nanotechnology definition (NSET, February 2000). February 2000.
[4] Mor GK, Shankar K, Paulose M, Varghese OK, Grimes CA. Use of Highly-Ordered TiO2 Nanotube Arrays in Dye-Sensitized Solar Cells. Nano Letters. 2005;6(2):215-218.
[5] Wang X, Zhi L, Mullen K. Transparent, Conductive Graphene Electrodes for Dye-Sensitized Solar Cells. Nano Letters. 2007;8(1):323-327.
[6] Yang X, Loos J, Veenstra SC, Verhees WJH, Wienk MM, Kroon JM, et al. Nanoscale Morphology of High-Performance Polymer Solar Cells. Nano Letters. 2005;5(4):579-583.
[7] Huynh WU, Dittmer JJ, Alivisatos AP. Hybrid Nanorod-Polymer Solar Cells. Science. 2002;295(5564):2425-2427.
[8] Ramakrishna S. An introduction to electrospinning and nanofibers. Singapore; Hackensack, NJ: World Scientific; 2005.
[9] Stephens JS, Chase DB, Rabolt JF. Effect of the Electrospinning Process on Polymer Crystallization Chain Conformation in Nylon-6 and Nylon-12. Macromolecules. 2004;37(3):877-881.
[10] Reneker DH, Yarin AL, Zussman E, Xu H. Electrospinning of Nanofibers from Polymer Solutions and Melts. In: Hassan Aref and Erik van der G, editor. Advances in Applied Mechanics: Elsevier; 2007. p. 43-346.
[11] Huang Z-M, Zhang YZ, Kotaki M, Ramakrishna S. A review on polymer nanofibers by electrospinning and their applications in nanocomposites. Composites Science and Technology. 2003;63(15):2223-2253.
[12] Nain AS, Wong JC, Amon C, Sitti M. Drawing suspended polymer micro-/nanofibers using glass micropipettes. Appl Phys Lett. 2006;89(18):183105/183101-183105/183103.
[13] Chen L. Next generation of electrospun textiles for chemical and biological protection and air filtration: MIT; 2009.
[14] T. Ondarçuhu, Joachim C. Drawing a single nanofibre over hundreds of microns. EPL (Europhysics Letters). 1998;42(2):215.
[15] Che G, Lakshmi BB, Martin CR, Fisher ER, Ruoff RS. Chemical Vapor Deposition Based Synthesis of Carbon Nanotubes and Nanofibers Using a Template Method. Chemistry of Materials. 1998;10(1):260-267.
[16] Ma PX, Zhang R. Synthetic nano-scale fibrous extracellular matrix. Journal of biomedical materials research. 1999;46(1):60-72.

[17] Liu G, Ding J, Qiao L, Guo A, Dymov BP, Gleeson JT, et al. Polystyrene-block-poly(2-cinnamoylethyl methacrylate) Nanofibers—Preparation, Characterization, and Liquid Crystalline Properties. Chemistry – A European Journal. 1999;5(9):2740-2749.
[18] Whitesides GM, Grzybowski B. Self-Assembly at All Scales. Science. 2002;295(5564):2418-2421.
[19] Terada D, Kobayashi H, Zhang K, Tiwari A, Yoshikawa C, Hanagata N. Transient charge-masking effect of applied voltage on electrospinning of pure chitosan nanofibers from aqueous solutions. Sci Technol Adv Mater. 2012;13(1):015003/015001-015003/015009.
[20] Yu JH. Electrospinning of polymeric nanofiber materials: Process characterization and unique applications: MIT; 2007.
[21] Kashiwagi T, Harris RH, Zhang X, Briber RM, Cipriano BH, Raghavan SR, et al. Flame retardant mechanism of polyamide 6-clay nanocomposites. Polymer. 2004;45(3):881-891.
[22] Morgan AB. Flame retarded polymer layered silicate nanocomposites: a review of commercial and open literature systems. Polymers for Advanced Technologies. 2006;17(4):206-217.
[23] Camino G, Fina A, Tabuani D. POSS as promising fire retardants in polymer nanocomposites. Rapra Technology Ltd.; 2006. p. P16/11-P16/16.
[24] Samyn F, Bourbigot S, Jama C, Bellayer S, Nazare S, Hull R, et al. Characterisation of the dispersion in polymer flame retarded nanocomposites. European Polymer Journal. 2008;44(6):1631-1641.
[25] Kandola BK, Nazare S, Horrocks AR. Thermal degradation behaviour of flame-retardant unsaturated polyester resins incorporating functionalised nanoclays. Royal Society of Chemistry; 2005. p. 147-160.
[26] Jang BN, Wilkie CA. The effect of clay on the thermal degradation of polyamide 6 in polyamide 6/clay nanocomposites. Polymer. 2005;46(10):3264-3274.
[27] Bourbigot S, Devaux E, Flambard X. Flammability of polyamide-6/clay hybrid nanocomposite textiles. Polymer Degradation and Stability. 2002;75(2):397-402.
[28] Dabrowski F, Le Bras M, Delobel R, Gilman JW, Kashiwagi T. Using clay in PA-based intumescent formulations. Fire performance and kinetic parameters. Macromolecular Symposia. 2003;194(1):201-206.
[29] Fornes TD, Yoon PJ, Hunter DL, Keskkula H, Paul DR. Effect of organoclay structure on nylon 6 nanocomposite morphology and properties. Polymer. 2002;43(22):5915-5933.
[30] Paul DR, Robeson LM. Polymer nanotechnology: Nanocomposites. Polymer. 2008;49(15):3187-3204.
[31] Ploehn HJ, Liu C. Quantitative Analysis of Montmorillonite Platelet Size by Atomic Force Microscopy. Industrial & Engineering Chemistry Research. 2006;45(21):7025-7034.
[32] Cho JW, Paul DR. Nylon 6 nanocomposites by melt compounding. Polymer. 2001;42(3):1083-1094.

[33] Lao SC, Yong W, Nguyen K, Moon TJ, Koo JH, Pilato L, et al. Flame-retardant polyamide 11 and 12 nanocomposites: processing, morphology, and mechanical properties. J Compos Mater. 2010;44(25):2933-2951.
[34] Lao SC, Wu C, Moon TJ, Koo JH, Morgan A, Pilato L, et al. Flame-retardant polyamide 11 and 12 nanocomposites: thermal and flammability properties. J Compos Mater. 2009;43(17):1803-1818.
[35] S. C. Lao, J. H. Koo, T. J. Moon, M. Londa, C. C. Ibeh, G. . Wissler, et al. Flame-retardant Polyamide 11 Nanocomposites: Further Thermal and Flammability Studies. J of Fire Sciences. 2011;29(6):479-498.
[36] Cloisite® 30B Typical Physical Properties Bulletin. SOUTHERN CLAY PRODUCTS; 2012. p. 2.
[37] Product datasheet OP1312. Clariant; 2011.
[38] Chavarria F, Shah RK, Hunter DL, Paul DR. Effect of melt processing conditions on the morphology and properties of nylon 6 nanocomposites. Polymer Engineering & Science. 2007;47(11):1847-1864.
[39] ASTM. D638-10. Standard Test Method for Tensile Properties of Plastics ASTM International2010.
[40] Fornes TD, Paul DR. Crystallization behavior of nylon 6 nanocomposites. Polymer. 2003;44(14):3945-3961.
[41] Usuki A, Koiwai A, Kojima Y, Kawasumi M, Okada A, Kurauchi T, et al. Interaction of nylon 6-clay surface and mechanical properties of nylon 6-clay hybrid. J Appl Polym Sci. 1995;55(1):119-123.
[42] Walters RN, Lyon RE. A Microscale Combustion Calorimeter. In: U.S. Department of Transportation FAA, National Technical Information Service, editor. Springfield, VA2003.
[43] Fong H, Liu W, Wang C-S, Vaia RA. Generation of electrospun fibers of nylon 6 and nylon 6-montmorillonite nanocomposite. Polymer. 2002;43(3):775-780.
[44] Koombhongse S, Liu W, Reneker DH. Flat polymer ribbons and other shapes by electrospinning. Journal of Polymer Science Part B: Polymer Physics. 2001;39(21):2598-2606.
[45] Deitzel JM, Kleinmeyer J, Harris D, Beck Tan NC. The effect of processing variables on the morphology of electrospun nanofibers and textiles. Polymer. 2001;42(1):261-272.
[46] Li L, Bellan LM, Craighead HG, Frey MW. Formation and properties of nylon-6 and nylon-6/montmorillonite composite nanofibers. Polymer. 2006;47(17):6208-6217.
[47] Brenier R. Bifunctional Surfaces with Superhydrophobic and Plasmonic Properties. The Journal of Physical Chemistry C. 2011;115(21):10544-10549.
[48] Yao X, Song Y, Jiang L. Applications of Bio-Inspired Special Wettable Surfaces. Advanced Materials. 2011;23(6):719-734.
[49] Tuteja A, Choi W, Ma M, Mabry JM, Mazzella SA, Rutledge GC, et al. Designing Superoleophobic Surfaces2007.

[50] Nosonovsky M, Bhushan B. Superhydrophobic surfaces and emerging applications: Non-adhesion, energy, green engineering. Current Opinion in Colloid & Interface Science. 2009;14(4):270-280.
[51] Bahners T, Textor T, Opwis K, Schollmeyer E. Recent Approaches to Highly Hydrophobic Textile Surfaces. Journal of Adhesion Science & Technology. 2008;22(3/4):285-309.
[52] Feng L, Li S, Li Y, Li H, Zhang L, Zhai J, et al. Super-hydrophobic surfaces: from natural to artificial. Adv Mater (Weinheim, Ger). 2002;14(24):1857-1860.
[53] Gao X, Jiang L. Biophysics: Water-repellent legs of water striders. Nature. 2004;432(7013):36-36.
[54] Ma M, Hill RM, Rutledge GC. A review of recent results on superhydrophobic materials based on micro- and nanofibers. J Adhes Sci Technol. 2008;22(15):1799-1817.
[55] Yin L, Zhu L, Wang Q, Ding J, Chen Q. Superhydrophobicity of Natural and Artificial Surfaces under Controlled Condensation Conditions. ACS Appl Mater Interfaces. 2011;3(4):1254-1260.
[56] Bhushan B, Jung YC. Natural and biomimetic artificial surfaces for superhydrophobicity, self-cleaning, low adhesion, and drag reduction. Progress in Materials Science. 2011;56(1):1-108.
[57] Kim SH. Fabrication of Superhydrophobic Surfaces. Journal of Adhesion Science and Technology. 2008;22:235-250.
[58] Ma M, Hill RM. Superhydrophobic surfaces. Current Opinion in Colloid & Interface Science. 2006;11(4):193-202.
[59] Nosonovsky M. Multiscale Roughness and Stability of Superhydrophobic Biomimetic Interfaces. Langmuir. 2007;23(6):3157-3161.
[60] Nakajima A, Hashimoto K, Watanabe T. Recent Studies on Super-Hydrophobic Films. Monatshefte für Chemie / Chemical Monthly. 2001;132(1):31-41-41.
[61] Guo Z, Liu W, Su B-L. Superhydrophobic surfaces: From natural to biomimetic to functional. Journal of Colloid and Interface Science. 2011;353(2):335-355.
[62] Shirtcliffe NJ, McHale G, Newton MI, Chabrol G, Perry CC. Dual-Scale Roughness Produces Unusually Water-Repellent Surfaces. Advanced Materials. 2004;16(21):1929-1932.
[63] Wang J, Liu F, Chen H, Chen D. Superhydrophobic behavior achieved from hydrophilic surfaces. Appl Phys Lett. 2009;95(8):084104/084101-084104/084103.
[64] Ming W, Wu D, van BR, de WG. Superhydrophobic Films from Raspberry-like Particles. Nano Lett. 2005;5(11):2298-2301.
[65] Hsu S-H, Sigmund WM. Artificial Hairy Surfaces with a Nearly Perfect Hydrophobic Response. Langmuir. 2010;26(3):1504-1506.
[66] Zhou Z, Liu X, Hu B, Wang J, Xin D, Wang Z, et al. Hydrophobic surface modification of ramie fibers with ethanol pretreatment and atmospheric pressure plasma treatment. Surface and Coatings Technology. 2011;205(17-18):4205-4210.
[67] Hoefnagels HF, Wu D, de With G, Ming W. Biomimetic Superhydrophobic and Highly Oleophobic Cotton Textiles. Langmuir. 2007;23(26):13158-13163.

[68] Han D, Steckl AJ. Superhydrophobic and Oleophobic Fibers by Coaxial Electrospinning. Langmuir. 2009;25(16):9454-9462.
[69] Ma M, Gupta M, Li Z, Zhai L, Gleason KK, Cohen RE, et al. Decorated Electrospun Fibers Exhibiting Superhydrophobicity. Advanced Materials. 2007;19(2):255-259.
[70] Chiou N-R, Lu C, Guan J, Lee LJ, Epstein AJ. Growth and alignment of polyaniline nanofibres with superhydrophobic, superhydrophilic and other properties. Nat Nano. 2007;2(6):354-357.
[71] Gao S-H, Gao L-H, Zhou K-S. Super-hydrophobicity and oleophobicity of silicone rubber modified by CF4 radio frequency plasma. Appl Surf Sci. 2011;257(11):4945-4950.
[72] Gao S-H, Lei M-K, Liu Y, Wen L-S. CF4 radio frequency plasma surface modification of silicone rubber for use as outdoor insulations. Applied Surface Science. 2009;255(11):6017-6023.
[73] Rauscher H, Perucca M, Buyle G. Plasma Technology for Hyperfunctional Surfaces : Food, Biomedical, and Textile Applications. Hoboken: Wiley-VCH; 2010.
[74] Woodward I, Schofield W, Roucoules V, Bradley T, Badyal J. Micropatterning of Plasma Fluorinated Super-hydrophobic Surfaces. Plasma Chemistry and Plasma Processing. 2006;26(5):507-516-516.
[75] Jiang T, Wang Y-h, Yeh J-t, Fan Z-q. Study on solvent permeation resistance properties of nylon6/clay nanocomposite. European Polymer Journal. 2005;41(3):459-466.